ORNL-3888
UC-34 – Physics

EFFICIENCY OF ORGANIC SCINTILLATORS FOR FAST NEUTRONS

R. J. Schuttler

N66 33434

FACILITY FORM 602

(ACCESSION NUMBER) (THRU)

71 (PAGES) 1 (CODE)

CR-76860 (NASA CR OR TMX OR AD NUMBER) 24 (CATEGORY)

GPO PRICE $ _____

CFSTI PRICE(S) $ _____

Hard copy (HC) 3.00

Microfiche (MF) .75

ff 653 July 65

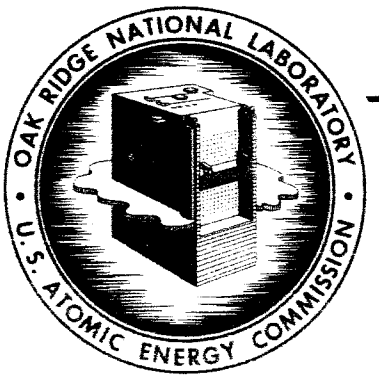

OAK RIDGE NATIONAL LABORATORY
operated by
UNION CARBIDE CORPORATION
for the
U.S. ATOMIC ENERGY COMMISSION

Printed in USA. Price $3.00 . Available from the Clearinghouse for Federal Scientific and Technical Information, National Bureau of Standards, U.S. Department of Commerce, Springfield, Virginia 22151

LEGAL NOTICE

This report was prepared as an account of Government sponsored work. Neither the United States, nor the Commission, nor any person acting on behalf of the Commission:

A. Makes any warranty or representation, expressed or implied, with respect to the accuracy, completeness, or usefulness of the information contained in this report, or that the use of any information, apparatus, method, or process disclosed in this report may not infringe privately owned rights; or

B. Assumes any liabilities with respect to the use of, or for damages resulting from the use of any information, apparatus, method, or process disclosed in this report.

As used in the above, "person acting on behalf of the Commission" includes any employee or contractor of the Commission, or employee of such contractor, to the extent that such employee or contractor of the Commission, or employee of such contractor prepares, disseminates, or provides access to, any information pursuant to his employment or contract with the Commission, or his employment with such contractor.

ORNL-3888

Contract No. W-7405-eng-26

Neutron Physics Division

EFFICIENCY OF ORGANIC SCINTILLATORS FOR FAST NEUTRONS

R. J. Schuttler*

NOTE:
This Work Supported by
NATIONAL AERONAUTICS AND SPACE ADMINISTRATION
Under Order R-104

JULY 1966

*Present address: Physique du Solide, University of Toulouse, France.

OAK RIDGE NATIONAL LABORATORY
Oak Ridge, Tennessee
operated by
UNION CARBIDE CORPORATION
for the
U.S. ATOMIC ENERGY COMMISSION

CONTENTS

NOMENCLATURE

η = efficiency, in counts/incident neutron

Σ_T = total macroscopic cross section

h = scintillator thickness

N_H = atomic density of hydrogen in the scintillator

= 0.04826×10^{24} atoms/cm^3 at 23°C

N_C = atomic density of carbon in the scintillator

= 0.03986×10^{24} atoms/cc at 23°C

$\sigma_{T,H}$ = free elastic-scattering microscopic cross section of hydrogen

$\sigma_{T,C}$ = total microscopic cross section of carbon

p = number of photoelectrons from multiplier photocathode, with subscripts referring to fast or total light

F = fast pseudoelectron equivalent (p.e.q.) energy

T = total p.e.q. energy

k = number of photoelectrons/MeV p.e.q.

B, B' = constants in the relation between energy loss and light output

E_o = energy of incident neutrons

ζ = ratio of the total number of photoelectrons in a pulse to the number in the fast component

b_F = descriminator bias in photons

$\Phi_F(E_o,F)$ = fast spectrum of the light output, in p.e.q.

ζ^* = effective ζ corresponding to the discriminator speed

E_B, ϵ_B = discriminator biases for a secondary particle, in units of MeV p.e.q. and of the secondary particles energy, respectively

k^* = k/ζ^*, a measure of the pulse height resolution

η_1, η_2 = first and second effective collision efficiencies

J_o = incident current of neutrons per cm^2

Φ_{i-1} = energy spectrum of the neutrons which have made i-1 collision

$g_H(E_o,E_B)$ = mean proportion of collisions of neutron with hydrogen or carbon which are detected above the bias E_B

$g_H(E_o,E_B)$ = mean proportion of collisions of neutrons with hydrogen or carbon which are detected above the bias E_B

μ = $\cos \theta_{c.m.}$

E_C = carbon recoil energy

A = atomic mass of carbon (neutron = 1)

Σ_R = macroscopic removal cross section

ρ = attenuated incident current, by the scintillator

h^* = effective thickness of scintillator

E_{psd}, ϵ_{psd} = upper biases in the pulse shape discrimination

R_o = range of a proton of E_o

r = scintillator radius

ψ = scattering angle of neutrons in the center-of-mass system

σ_θ = angular differential cross section for n-p scattering

w = energy differential microscopic cross section

W = energy differential macroscopic cross section

Σ^{eff}, σ^{eff} = effective macroscopic and microscopic cross section for a given bias E_B

Σ_1^{eff} = effective macroscopic cross section for the first collision

$\Sigma_{2,H}^{eff}$ = effective macroscopic cross section for the second collision

v_C = velocity of compound nucleus before decay

v_ϵ^2 = $\frac{2\epsilon}{m}$ = squared channel velocity

E_S = separation energy

$\varphi(F)$ = the p.e.q. energy spectrum of the fraction of the carbon geometrical cross section which leads to detection by the cascade pulse evaporation process

c = velocity of light

Σ_g = macroscopic geometrical cross section

$V_{c.m.}$ = center-of-mass velocity in the $C^{12}(n,\alpha)Be^9$

M_n = neutron mass

M_B = mass of ^9Be atom

$J_1(x)$ = straight ahead current of neutrons after first effective collision

ω = ratio which expresses the importance of the forward-peaked flux from carbon inelastic scattering

Σ_t = transport cross section which is the sum of hydrogen scatters and inelastic scattering on carbon leading to the 4.4 MeV level

EFFICIENCY OF ORGANIC SCINTILLATORS FOR FAST NEUTRONS*

R. J. Schuttler†

N66-33434

ABSTRACT

Organic scintillator detection efficiencies are estimated for incident neutrons above 12 MeV, in which region nonelastic reactions in the carbon of the detector become significant. The efficiency is given in a "first effective collision" approximation, later corrected for second-collision effects, as a function of a detector threshold on the fast component of the light from the phosphor. The analysis includes consideration of nonlinear light production of both fast- and slow-light components, pulse-shape discrimination against gamma rays, the detector's pulse-height resolution, and edge effects. Effective carbon cross sections are approximated by combining a Monte Carlo intranuclear cascade and evaporation contribution with the experimental $^{12}C(n,\alpha)^{9}Be$ cross section. Pulse heights are summed from the series of particles emitted in the reaction of a given incident neutron with a carbon nucleus, including pulses from secondary neutron interactions. For 14.5-MeV incident neutrons onto NE-213 detectors 2.61 and 6.1 cm thick, the method yields efficiencies of 9.7 and 21.7% for a fast-light threshold equivalent to pulses from 200-keV electrons, if no pulse-shape discrimination against gamma rays is employed.

Author

I. INTRODUCTION

Some calculations have already been made for determining the fast-neutron efficiency of organic scintillators.[1-5‡] However, with the exception of the paper by Kurz,[5] most of the emphasis has been on the determination of the efficiency below 15 MeV, where the problem of multiple scattering is relatively more important than for high energy.

The work reported here was initiated in an effort to provide calculated absolute detector efficiencies for an experiment involving spectra

*Work funded by the National Aeronautics and Space Administration under NASA Order R-104. This report was completed and edited after Dr. Schuttler's visit to the Laboratory was completed, and though he cooperated greatly in its final production it is possible that his intentions have not been precisely represented. We thank him for his continued efforts, and hope there have been no serious misinterpretations.

†Present address: Physique du Solide, University of Toulouse, France.

‡See List of References at end of report.

of secondary neutrons from 160-MeV protons on various nuclei,[6] and so the particular examples worked out where chosen to fit the parameters of that experiment. The experiment employed disk-shaped detectors with the neutrons impinging parallel to the symmetry axis, a threshold discriminator consisting of a tunnel diode univibrator which responded only to the fast light from the phosphor, and a pulse-shape discrimination system based on the crossover point of a bipolar pulse from a slow amplifier system, which therefore responded approximately to the ratio of slow to total light emitted.

Certain problems were involved in the calculation. Since scintillators are sensitive only to charged particles, neutrons must be converted by means of a radiator, as abstractly shown in Fig. 1. In experiments in which the radiator and the scintillator are distinct, such as those reported in Refs. 7-8, a pure-hydrogen radiator can be used and the detector can be shielded. However, since such an apparatus has a very poor efficiency ($\sim 10^{-5}$) and is difficult to use in time-of-flight experiments, my interest was in the use of an organic scintillator as both radiator and detector. The lower limit of use can be as low as 50 keV (Ref. 10) and the efficiency (i.e., η, the ratio of the number of counts to the number of incident neutrons) can be as high as 35%. Large scintillators have been studied for use at higher energies.[9]

Some emphasis is now being placed on the use of liquid scintillators which have good transparency, and all the data reported here are for the liquid scintillator NE-213 (Nuclear Enterprises). Also, for some liquid scintillators, the pulses coming from heavy particles (protons, alphas, and other products of neutron reactions) can be well separated from the pulses coming from Compton electrons.[11] The main difficulty with using such detectors in spectrometry experiments is the determination of the efficiency vs the neutron energy. If there were no noise in the detection system, all events occuring in the scintillator could be counted, and the efficiency for neutrons striking the face of a scintillator slab would be equal in a plane geometry to the absorption:

$$\eta = \eta_{max} = 1 - \exp\left(-\Sigma_T h\right) , \qquad (1)$$

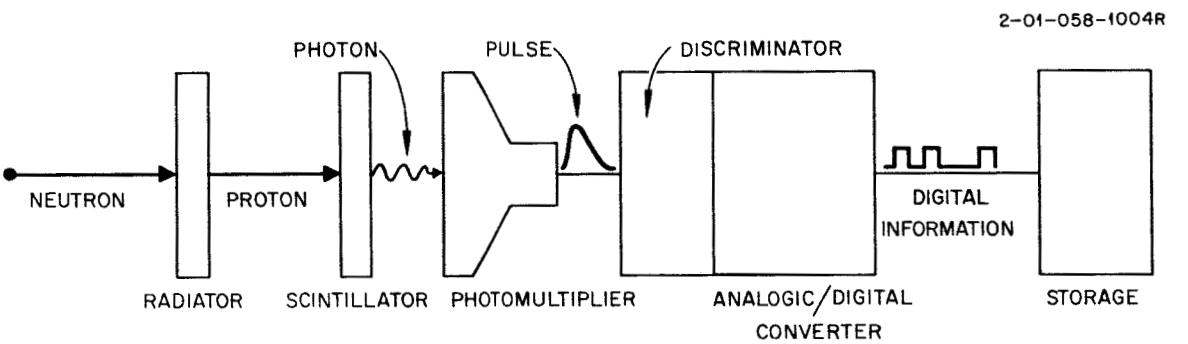

Fig. 1. Principle of Neutron Detection by Proton Recoil.

where h is the thickness of the scintillator and Σ_T is the total macroscopic cross section. Since organic scintillators are composed principally of hydrogen and carbon,

$$\Sigma_T = N_H \sigma_{T,H} + N_C \sigma_{T,C} , \qquad (2)$$

where N_H and N_C are respectively the number of atoms of hydrogen and carbon per cubic centimeter, and $\sigma_{T,H}$ and $\sigma_{T,C}$ are their microscopic total cross sections. Figure 2 shows the maximum efficiency for two typical scintillators. However, for handling (and storing) the data, the detection system must have a threshold for discriminating valid pulses from noise, which can include the gamma rays detected by the scintillator. With this inclusion the electronic equipment begins to be very complex, and this complexity is reflected in the calculation of the efficiency. If we assume good linearity and constant gain in the photomultiplier tube, we can consider that the analyzing equipment works directly with the light output of each event. However, to take into account the neutron vs gamma discrimination, we have to observe how the light is emitted vs time.

II. LIGHT OUTPUT EQUIVALENTS

If t = 0 is the time when nuclear reactions and the slowing down of the charged particles occur (these processes require less than 10^{-16} and 10^{-12} sec, respectively), we can measure the amount of "fast" light (and photoelectrons, p_F) emitted by all the charged particles between t = 0 and a fixed value t_F ($\sim$5 nsec). We can do the same thing for the "total" light between 0 and t_T ($\gg$ 1 μsec; practical considerations often require that t_T be chosen in the vicinity of 1 μsec), which gives p_T. Figure 3 illustrates the time dependence of the photoelectron emission rate. Discrimination between electrons and protons is possible on the basis of light emission because p_F/p_T is a function of the specific energy loss of a particle. (The relation between these quantities and the energy and the stopping power of the incident charged particle is described in another paper.[12])

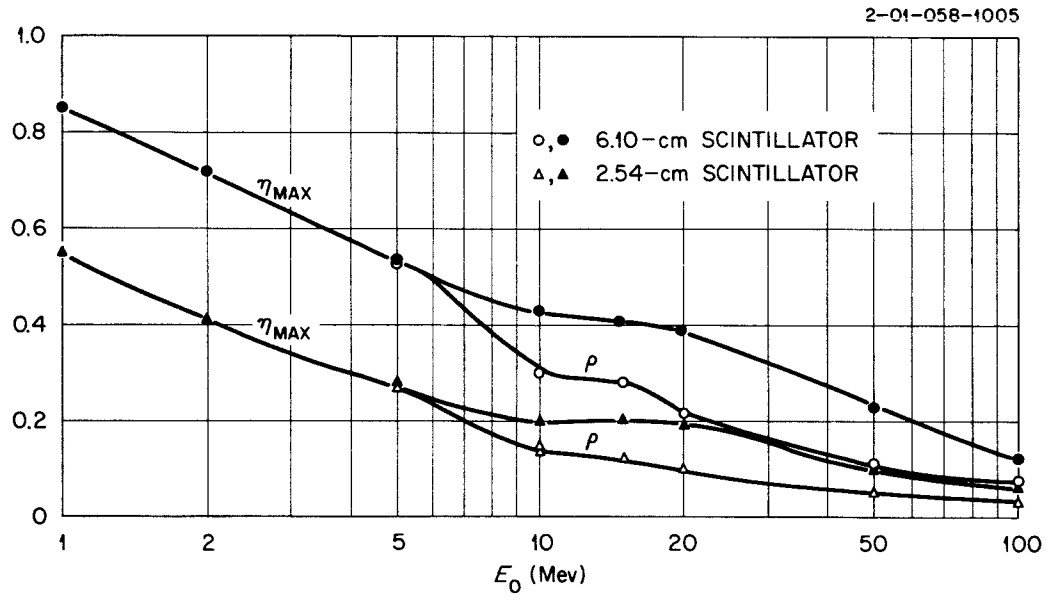

Fig. 2. Maximum (Zero Bias) Efficiency η_{max} and Attenuated Primary Neutron Current $\rho = 1 - e^{-\Sigma_R h}$ vs Neutron Energy E_o for Scintillator Thicknesses 2.54 and 6.10 cm.

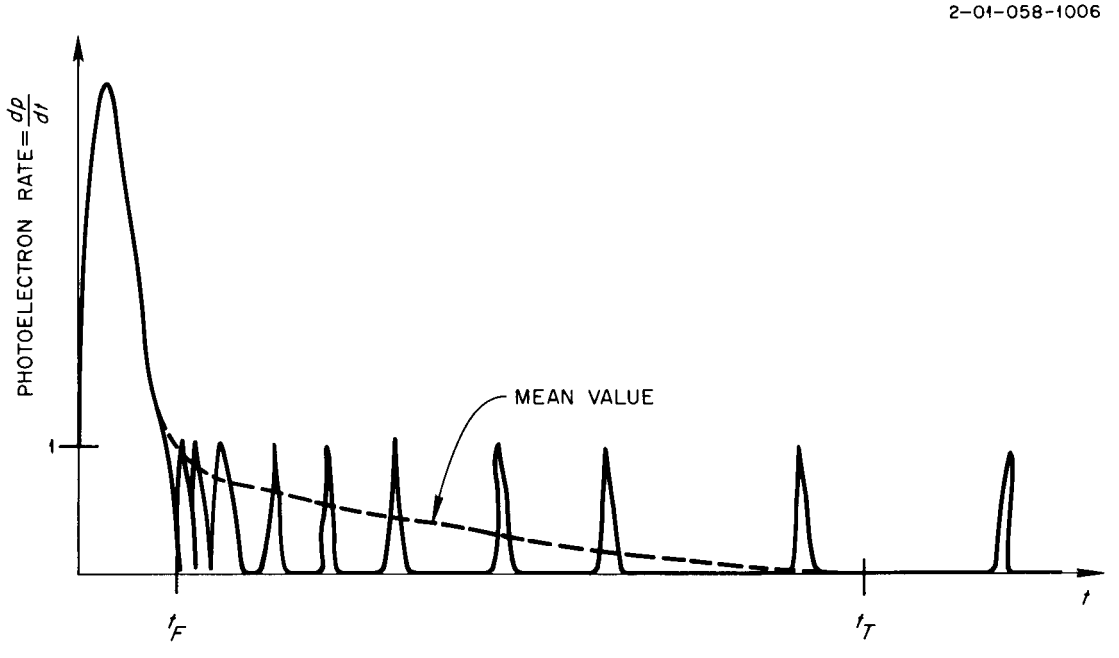

Fig. 3. Photoelectron Emission Rate from an Organic Phosphor as Seen by a Fast Oscilloscope. $t_F \cong 5$ nsec, $t_T \cong 0.7$ μsec.

It is useful to measure fast- and slow-light production not in number of photons but in electron-equivalent energy, i.e., the energy of an electron giving the same mean amount of light. (As seen below, it is actually necessary to use a hypothetical electron whose specific energy loss is vanishingly small to avoid quenching of the light.) The measured quantities are referred to as F and T. Due to the quantum nature of the light emission and of the photoelectric effect, electrons of energy F yield a spectrum of values $P_F(p_F)$. Only a proportionality between the average value $\bar{p}_F$ (or $\bar{p}_T$) and F (or T) can be assumed, and so the frequency function Eq. (3) is employed for the number of "effective" photoelectrons from an absorption of F keV:

$$P_F(p_F) = \left(\frac{1}{\sqrt{2\pi kF}}\right) \exp\left[-\frac{(p_F - kF)^2}{2kF}\right], \tag{3}$$

where k = "effective" number of photoelectrons per MeV so that $\langle p_F \rangle = kF$, where the angle brackets indicate the mean value. Equation (3) assumes a normal approximation to the Poisson distribution of photoelectrons. The use of the electron equivalent enables us to compute the light output of a charged particle with a perfect "scintibloc" (scintillator plus the photomultiplier) and to calibrate the scintibloc gain with a gamma-ray source.

The relation between the total-light output T and the energy of charged particles has been thoroughly studied.[13-23] However, it should be noted that, except in some recent work,[22] experimenters try to fit the data from the total-light output with the semiempirical law given by Birks[20] for the fast output:

$$\frac{dF}{dE} = \frac{1}{1 + B\frac{dE}{dx}}. \tag{4}$$

This formula assumes that F, measured in electron equivalents, is on the average proportional to p_F, an assumption which neglects the variable energy loss of electrons. Actually (see Table 1) a little quenching reduces the light output of electrons below 100 keV. This effect

Table 1. Energy Loss of Charged Particles in NE-213[a]

Particle	Energy (MeV)	dE/dx (MeV $cm^2 g^{-1}$)	Range (mg/cm^2)
Electron[b]	0.01	23.0[d]	2.3
	0.1	4.15	14.0
	10.0	1.96	5,180.0
Proton[c]	0.06	1,090.0[d]	0.1
	1.0	277.0	2.2
	10.0	47.0	119.0
	85.0	8.3	5,700.0
Alpha[c]	0.5	2,840.0[d]	0.7
	2.0	1,800.0	1.3
	4.76	971.0	3.6
	6.11	811.0	7.2
Carbon nucleus	6.0	7,600.0[d]	
	12.0	5,300.0[e]	2.1
	36.0	4,000.0[e]	9.0
	60.0	2,900.0[e]	

[a]Composition: $N_H = 0.04826 \times 10^{24}$ atoms/cm^3, $N_C = 0.03986 \times 10^{24}$ atoms/cm^3, d = 0.8759 g/cm^3.

[b]Data from P. E. Schambra and A. M. Rauth, Phys. Rev. 120, 1758 (1960) and A. T. Nelms, Supplement to NBS-377 (1958).

[c]Using a mixture of toluene and xylene, I = 59.4 eV, data were computed according to the method described by R. W. Peelle, Rapid Computation of Specific Energy Losses for Energetic Charged Particles, TM-977 (Apr. 29, 1965).

[d]Maximum value.

[e]Experimental data from P. E. Schambra and A. M. Rauth, Phys. Rev. 120, 1758 (1960).

can be taken into account in one of two ways: (1) Introduce a constant $A \neq 1$, which leads to the formula $dF/dE = A(1 + B\ dE/dx)^{-1}$, where A-1 is some mean value of B dE/dx for electrons in the range of measurement used so that dF/dE for electrons would be about unity; A-1 would be < 5% for electrons only if F were > 100 keV. (2) Use for the light output me measurement a "pseudoelectron equivalent" (p.e.q.), i.e., the energy of an electron giving the same mean amount of light in a hypothetical scintillator where no quenching occurs. This approach seems preferable.

When the scintillator is calibrated with real electrons, it is important to convert the energy of electrons to the slightly smaller energy of a pseudoelectron. An analysis of some of our experiments and a least-squares fit of the alpha-particle data of Flynn[21] enabled us to obtain light-output relations for the NE-213 liquid scintillator. The fast-light output measured in p.e.q. is given by an integral of Birks' law [Eq. (4)] with a value $B = 0.0140$ g cm^{-2} MeV^{-1}, which is somewhat higher than that used by others.[22] The total-light output is given by the relation

$$T = (1 - R)\ F + R\ S\ , \tag{5}$$

where $R = 0.15\ Z$ (found empirically)* and S is the equivalent slow-light output given by the integral of

$$\frac{dS}{dE} = \begin{cases} \exp\ (-B'\ dE/dx) & E > E_{cut} \\ 0 & E \leq E_{cut} \end{cases} \tag{6}$$

The cutoff energy E_{cut} was taken as half of the energy at which the maximum dE/dx occurs, and B′ was found to be = 0.0014 g cm^{-2} MeV^{-1}. This cutoff is introduced because at very low energy the energy loss is not entirely due to inelastic collisions with electrons. Some other processes such as radiation damage effects, can be significant. See J. Lindhard et al. [Kgl. Danske Videnskab. Selskab Mat. Fys. Medd. Vol. 33, No. 10 (1963)] for a computation of these effects.

*Later work indicates that a better fit can be obtained without assuming R to be a function of Z.

III. PRINCIPLE OF THE EFFICIENCY CALCULATION

A neutron can be detected only if it reacts to yield at least one charged particle, if $p_F > b_F$ (threshold of detection), and if

$$\zeta = \frac{p_T}{p_F} > \gamma \text{ (discrimination of nature)} . \tag{7}$$

The second condition depends on the use of a fast discriminator to set the detection threshold, and the third condition assumes that the pulse-shape discrimination system used depends on the ratio of slow to total light.

The fast-light output of a beam of monoenergetic neutrons gives a photoelectron spectrum, $S_F(p, E_o)$ (or S_T for the total-light spectrum). $S_F(p, E_o)dp$ is the probability of p being found between p and p + dp for an incident neutron of energy E_o.

Assuming a perfect neutron/gamma discrimination, the efficiency is now a function of b_F (or of its value in p.e.q.: E_B):

$$\eta(E_o,b_F) = \eta(E_o,E_B) = \int_o^\infty dp \int_o^\infty \frac{\Phi_F(E_o,F)dF}{\sqrt{2\pi kF}} \exp\left[-\frac{(p - kF)^2}{2kF}\right] \operatorname{erfc}\left[\sqrt{\frac{1}{kF\zeta^*}}\,(kE_B - p)\right] , \tag{8}$$

where $\Phi_F(E_o,F)$ is the "fast spectrum" of the light output, measured in p.e.q. for a perfect scintibloc, and where ζ^* is the effective ζ corresponding to the discriminator speed. erfc(q) is the complementary error function defined to give integrals of the normal distribution; it is zero for large positive q and unity for large negative q; erfc(0) = $\frac{1}{2}$, and erfc(1) = 0.16.

The problem now of relating $\Phi_F(E_o,F)$ to the cross section is very complex since for heavy particles (protons, alphas) F is not at all proportional to the kinetic energy ϵ. So not only do we have to know the total cross section for each type of reaction but also its energy spectrum, $\sigma(E_o \rightarrow \epsilon', \epsilon'', \ldots)$, where ϵ' ... are the energies of each particle emitted. If two particles of the same type are emitted

(two α's for example), the mean value of their light emission is not the same as it would be for a single particle with the same total energy. Another consequence is that twofold interactions have to be taken into account with some care.

This kind of analysis leads to the use of the Monte Carlo method to predict the energy distribution of the emitted charged particles, assuming that we have a good nuclear model of the interaction of neutrons with the nucleus. Since liquid scintillators contain only hydrogen and carbon, it is the uncertainty of our model for the carbon nucleus which is expected to give the major error in our calculation.

Since the efficiency of the scintillator is poor for the high-energy gamma rays emitted from de-excitation of the ^{12}C (for example, 0.1 for a 2.54-cm-thick scintillator, $E_\gamma = 4.43$ MeV), an examination of the cross sections (Fig. 4) shows that for neutron energies below 12 MeV the only charged particles which need be taken into account are the recoil nuclei (protons or carbon). Thus the efficiency can be calculated in this range by using a general neutron transport code. The purpose of the present calculation will be to calculate for neutrons above 12 MeV.

IV. FIRST-EFFECTIVE-COLLISION APPROXIMATION

At these energies η_{max}, which is equal to the probability that the neutron will have at least one collision in the scintillator, is relatively small compared with 1. So in the method of calculation which consists of decomposition of η into a series of contributions,

$$\eta = \eta_1 + \eta_2 + \eta_3 + \cdots + \eta_i \cdots , \tag{9}$$

η_1 is the efficiency calculated with only the first collision. Similarly, η_2 is calculated by following the neutrons which are not detected by their first collision to add the light output of any second collision, and so on. The series should converge fairly rapidly.

Each η_i is in turn the sum of two terms, according to whether the ith collision is on hydrogen or carbon, and we can write in the straightahead approximation

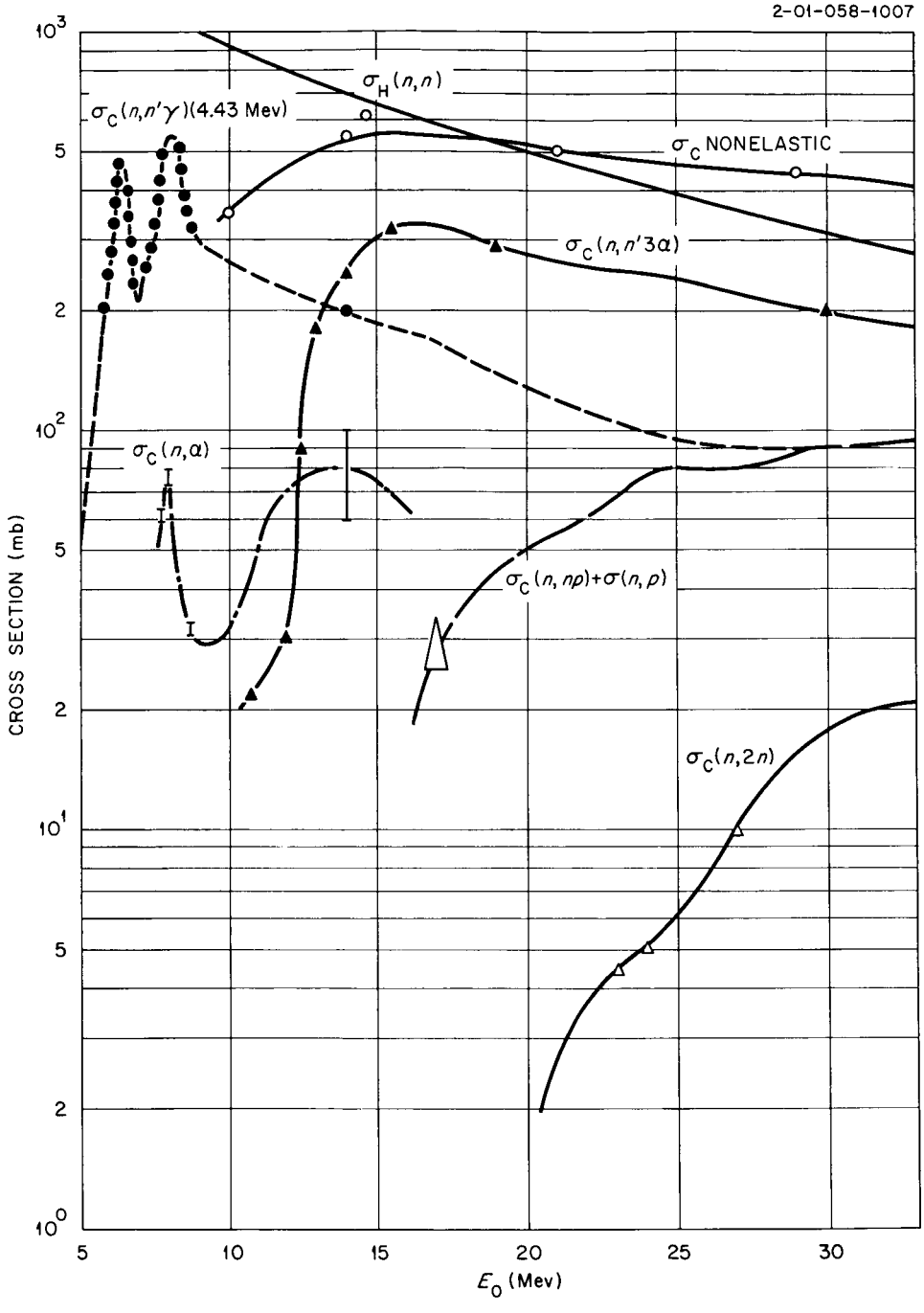

Fig. 4. Summary of Carbon Cross-Section Data for a NE-213 Scintillator. Data from D. J. Hughes and R. S. Schwartz, Neutron Cross Sections, BNL-325, Vol. I, 2d. ed. (July 1958), E. A. Davis et al., "Disintegration of O^{16} and C^{12} by Fast Neutrons," submitted for publication to Nuclear Physics, and M. L. Chatterjee and B. Sen, Nucl. Phys. 51, 583 (1964).

$$\eta_i = \frac{1}{J_o} \int_o^h dx \int_o^{E_o} \Phi_{i-1}(x,E) \times$$

$$\times \left[N_H \, \sigma_H(E) \, g_{iH}(E,E_B) + N_C \, \sigma_{C,T}(E) \, g_{iC}(E,E_B) \right] dE \, , \quad (10)$$

where J_o is the incident current of neutron energy E_o; $g_i(E,E_B)$ is the mean proportion of collisions detected with a bias E_B (in p.e.q.) for the target element indicated by the subscript; and Φ_{i-1} is the energy spectrum of neutrons which have made (i-1) collisions.

Φ_o may be written as

$$\Phi_o = J(x) \, \delta(E-E_o) \, . \quad (11)$$

Integrating over energy, the first-collision efficiency becomes

$$\eta_1 = \left[N_H \, \sigma_H(E_o) \, g_H(E_o,E_B) + N_C \, \sigma_{C,T}(E_o) \, g_C(E_o,E_B) \right] \times$$

$$\times \left[\frac{1}{J_o} \int_o^h J(x) \, dx \right] . \quad (12)$$

$J(x)$, the current of neutrons which have had no collisions, may be written as $J(x) = J_o \exp(-\Sigma_T x)$, consistent with the above definitions. As will be seen below, Σ_T is too large a cross section for practical purposes because elastic collisions with carbon have little effect.

At this point the definition of η_1 and η_2 is modified to assure that $\eta_2 \ll \eta_1$, even if Σh is large. The following types of first collision should be considered:

1. If it is with a proton, the neutron either gives a contribution to η_1 or is included in η_2.

2. If it is a nonelastic collision with a carbon nucleus, the neutron should be considered as being removed from the incident beam since any secondary neutron will have different energy and angle.

3. If it is an elastic collision with a carbon nucleus, there is little probability of detection. Figure 5 shows the differential cross section for the carbon nucleus vs 1-μ, where $\mu = \cos\theta_{c.m.}$. The

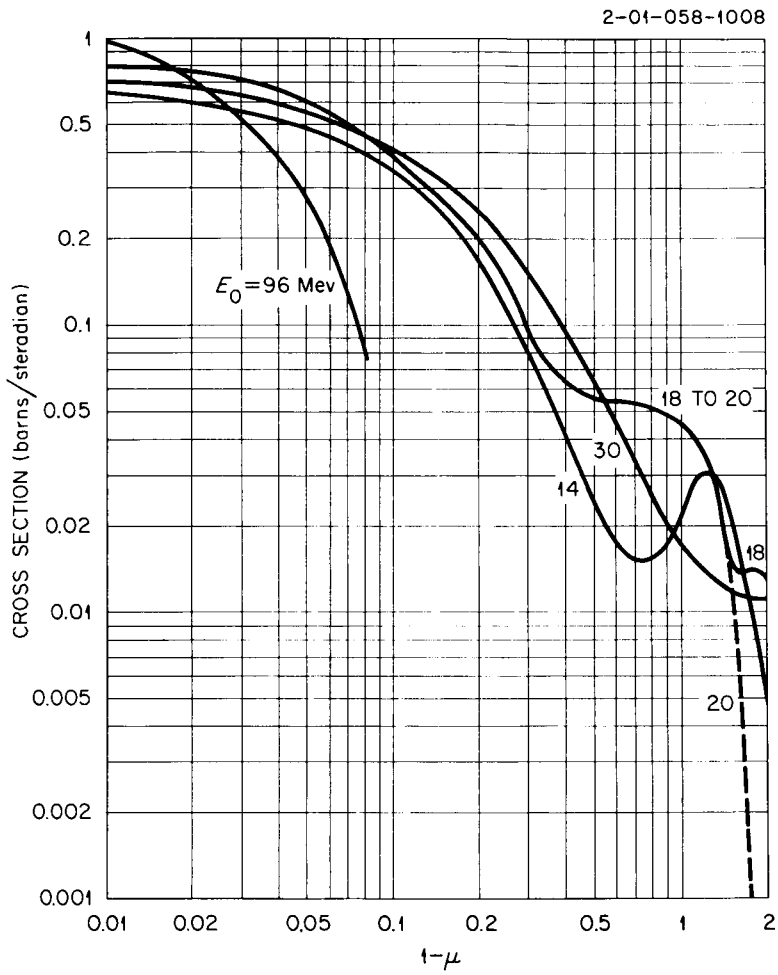

Fig. 5. Differential Cross Section for Elastic Scattering of Neutrons on Carbon vs 1 - μ. Data from J. D. Hughes and R. S. Carter, Neutron Cross Sections Angular Distributions, BNL-400 (June 1956) and M. V. Harlow, Jr., The Yield of Elastically Scattered 17- to 21-MeV Neutrons from the Reaction $C^{12}(n,n)C^{12}$, ORNL-3615 (June 1964).

abscissa is, consequently, proportional to the recoil energy:

$$E_C = \frac{2A}{(A+1)^2} E_o(1-\mu) \ . \qquad (13)$$

Since the recoil energy is generally small, the elastically scattered neutron will be considered as remaining in the primary beam.

Using the revised definition of a collison, the current of uncollided neutrons is written

$$J(x) = J_o \exp(\Sigma_R x) \ , \qquad (14)$$

where the removal cross section $\Sigma_R = N_H \sigma_H + N_C \sigma_{ne}$. This quantity is plotted in Fig. 6. The curves giving the attenuation ρ vs energy are plotted in Fig. 2, where $\rho = [1 - \exp(-\Sigma_R h)]$. It can be noted that the attenuation is always less than 30% above 12 MeV.

The last bracketed terms in Eq. (12) is called the "effective thickness" h*:

$$h^* = \frac{1}{J_o} \int_o^h J(x)\, dx = [1 - \exp(-\Sigma_R h)]/\Sigma_R \ . \qquad (15)$$

Figure 7 shows how h*/h varies with E_o. Note that this correction can be as high as 15% for a 6-cm detector. The use of the removal cross section to obtain J(x) has led us to an approximation where the behavior of the calculated efficiency depends mainly on the first collision; this method is called the "first-effective-collision approximation."

V. EDGE EFFECTS

The low value of bias contemplated here, about 180 keV p.e.q., leads us to neglect edge effects in the first analysis. However, the low specific energy loss of high-energy protons (14 MeV and above; see Table 1) is increasingly like that of electrons. To avoid erroneous pulse-shape discrimination (psd), which would have led to rejection of high-energy protons, another pulse-height bias was introduced, E_{psd}, above which every pulse was accepted as neutron-induced,

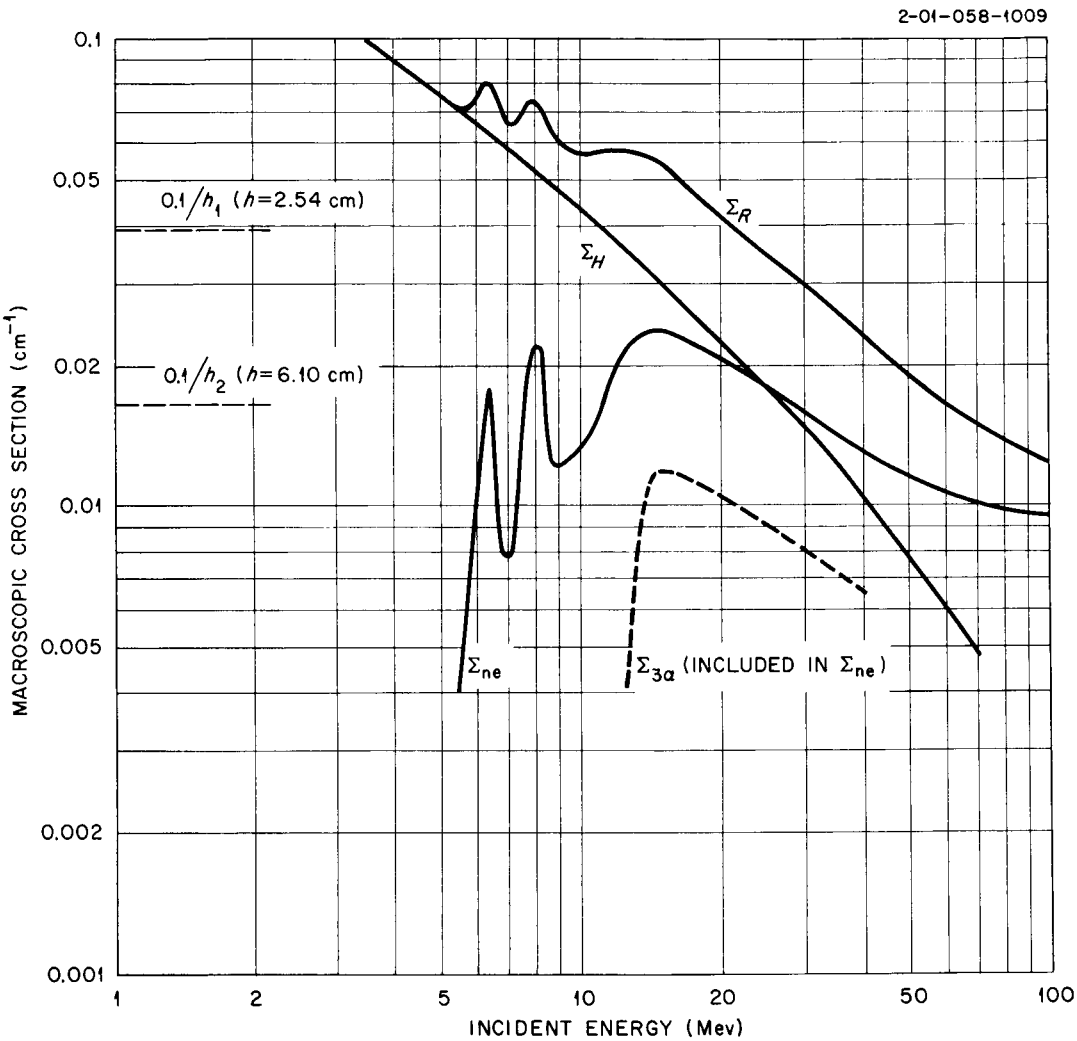

Fig. 6. Macroscopic Cross Sections of Reactions in Liquid Scintillator Which Remove Neutrons from the Incident Current.

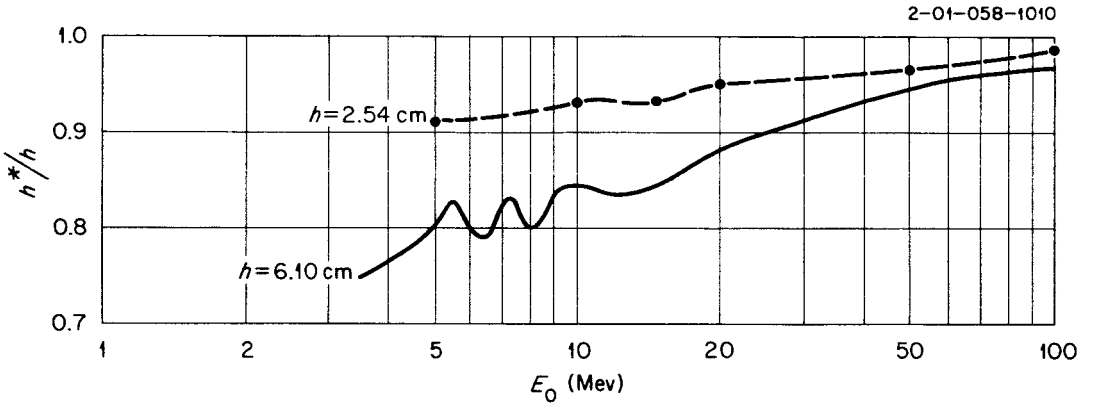

Fig. 7. Relative Effective Thickness $h^*/h = (1/\Sigma_R h)(1 - e^{-\Sigma_R h})$ Giving the Absorption Correction vs Neutron Energy.

independent of ζ. Therefore escaping protons emerging from the scintillator will always be counted if their total light output is above E_{psd} because their total energy loss is above an energy-dependent value of

$$\epsilon_{psd} = E_{psd}\left[1+B\left(\overline{\frac{dE}{dx}}\right)\right]. \tag{16}$$

For a reasonable value of E_{psd} = 2.5 MeV, ϵ_{psd} varies between 2.5 and 4 MeV.

An approximate evaluation of the loss of efficiency from edge effect is described by Rybakov and Sidorov.[24] The loss relative to the unbiased hydrogen efficiency is

$$\left(\frac{\Delta\eta}{\eta}\right)_{edge} = \frac{R_o}{h} D\left(\frac{\epsilon_{psd}}{E_o}\right) + \frac{R_o}{r} T\left(\frac{\epsilon_{psd}}{E_o}\right), \tag{17}$$

where R_o is the range of a proton of energy E_o, D and T are functions tabulated by Rossi and Staub,[25] and h and r are the thickness and the radius of the scintillator, respectively. Figure 8 gives the results of these calculations and it can be seen that this correction, with only the first term considered, is less than 5% at E_o = 100 MeV for a scintillator with h = 6.10 cm but could be 7% at E_o = 50 MeV if h = 2.54 cm. As shown later, the ranges of particles emitted in reactions of neutrons with the carbon nuclei are much less than the range of n-p protons, and so the edge effect loss for the nonelastic reactions on carbon can be neglected completely. Also, the pulses from this origin with pulse height below E_{psd} are likely in any case to satisfy the pulse-shape discrimination criterion.

VI. ANISOTROPY IN n,p SCATTERING

Above 10 MeV the scattering is not isotropic in the center-of-mass system. Gammel's formula[26] approximates the observed scattering:

$$\sigma_\psi = \frac{\sigma}{4\pi} \frac{1+2\left(\frac{E_o}{90}\right)^2 \cos^2\psi}{1+\frac{2}{3}\left(\frac{E_o}{90}\right)^2}, \tag{18}$$

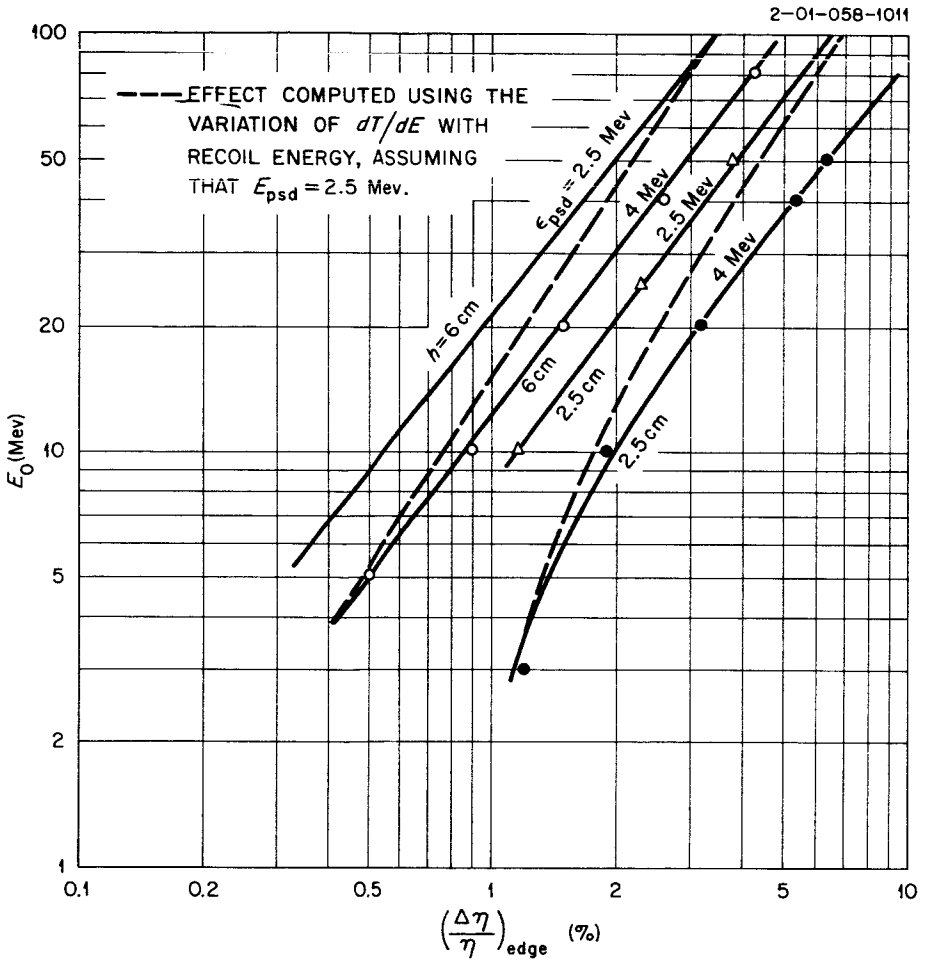

Fig. 8. Relative Edge Effect, Calculated for Protons Only. The dashed curves interpolate for a given electronic bias the calculations made for a given proton bias.

where ψ = scattering angle of neutrons in the center-of-mass system, and

$$\sigma = \frac{3\pi}{1.206\ E_o+(-1.8600+0.09415\ E_o+0.000130\ E_o^2)^2} + \\ + \frac{\pi}{1.206\ E_o+(0.4223+0.1300\ E_o)^2} \quad (19)$$

$$\simeq \frac{4.83}{\sqrt{E_o}} - 0.578 \text{ barn} \cdot \quad (20)$$

In the laboratory system,

$$E_p = \tfrac{1}{2}\ E_o\ (1-\cos\ \psi) \quad (21)$$

and

$$\sigma_\theta(\text{lab}) = 4\ \sigma_\psi\ \cos\ \theta\ . \quad (22)$$

The probability that a scattered neutron gives a proton in the range E_p, E_p+dE_p is

$$w(E_p)\ dE_p = \frac{4\pi\ \sigma_\psi}{\sigma} \times \frac{dE_p}{E_o}\ . \quad (23)$$

The differential macroscopic cross section is plotted in Fig. 9 as

$$W_H(E_p) = N_H\ \sigma\ w(E_p)\ . \quad (24)$$

If the bias is sufficiently low, Eqs. (9) through (12) can be simplified with respect to the contribution of hydrogen to the efficiency:

$$\eta(E_o,\ E_B) = h^* \int_{\epsilon_B}^{\infty} W_H(E_p)\ dE_p = h^*\ \Sigma(E_o,\ \epsilon_B)\ , \quad (25)$$

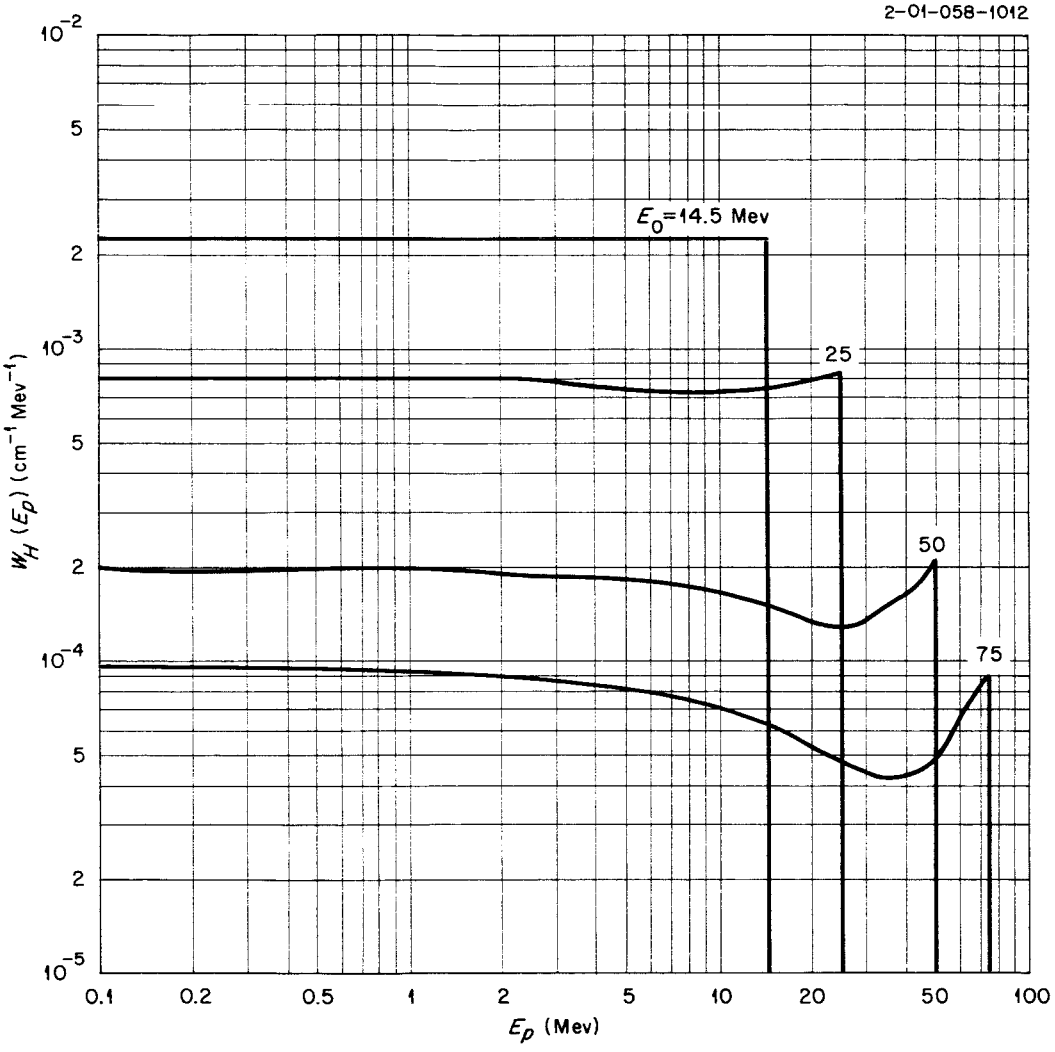

Fig. 9. Proton Energy Differential Macroscopic Cross Section for Elastic Scattering on Hydrogen, $W_H(E_p)$.

where h* is the effective thickness of the scintillator. With the same assumption, the effective macroscopic cross section for hydrogen reactions can be written as

$$\Sigma_H^{eff} = \Sigma(E_o, \epsilon_B) = \Sigma_H\left[1-\alpha(E_o)\frac{\epsilon_B}{E_o}\right] . \qquad (26)$$

Table 2 gives some values of Σ_H and $\alpha = \frac{4\pi\sigma_{\psi=0}}{\sigma}$, which is the (forward/average) anisotropy coefficient. Figure 10 shows the curves of Σ vs E_o for ϵ_B = 0 and 1 MeV (i.e., E_B = 180 keV).

VII. DETECTION OF CARBON RECOIL NUCLEI

The differential elastic cross section for carbon is not very well known. However, it is important to recognize that there is a very strong forward lobe (see Fig. 5). Consequently the recoil kinetic energy is on the average very low:

$$E_C = \frac{2A\ E_o(1-\cos\psi)}{(A+1)^2} = 0.142\ E_o(1-\cos\psi) , \qquad (27)$$

where ψ = the scattering angle in the center-of-mass system. Figure 11 shows the differential cross section as a function of the recoil kinetic energy. We again define the differential efficiency as

$$W_C(E_C) = N_C\ \sigma_{el}\ w(E_C) , \qquad (28)$$

where $w(E_C)$ has a similar meaning to $w(E_p)$ in Eq. (20):

$$w(E_C) = \frac{4\mu\sigma(\psi)}{\sigma} \times \frac{1}{E_C^{max}} . \qquad (29)$$

Scaling the ordinate of Fig. 11 easily transforms each curve into a plot of $W_C(E_C)$, but to determine the fast-light distribution of the fraction of the geometrical cross section which contributes to the efficiency, $\Phi(F)$, the relations for $F(E_C)$ are needed. Batchelor[1]

Table 2. Macroscopic Cross Section, Anisotropy Coefficient, α, and Resultant Bias Effect for Detection of Neutrons by Proton Recoil

E_o (MeV)	Σ_H (cm^{-1})	α	$\Sigma(E_o, \epsilon_B = 1\ MeV)$ (cm^{-1})	Relative Loss (%) of Efficiency from Bias Effect
14.5	0.03233	1.0343	0.0300	7.11
20.0	0.02342	1.0637	0.0222	5.32
25.0	0.01840	1.0978	0.0176	4.39
30.0	0.01499	1.1379	0.0144	3.79
40.0	0.01060	1.2327	0.0103	3.08
50.0	0.00794	1.3413	0.00772	2.68
60.0	0.006185	1.4571	0.00602	2.43
75.0	0.00447	1.6329	0.00436	2.18
90.0	0.00337	1.8000	0.00328	2.00

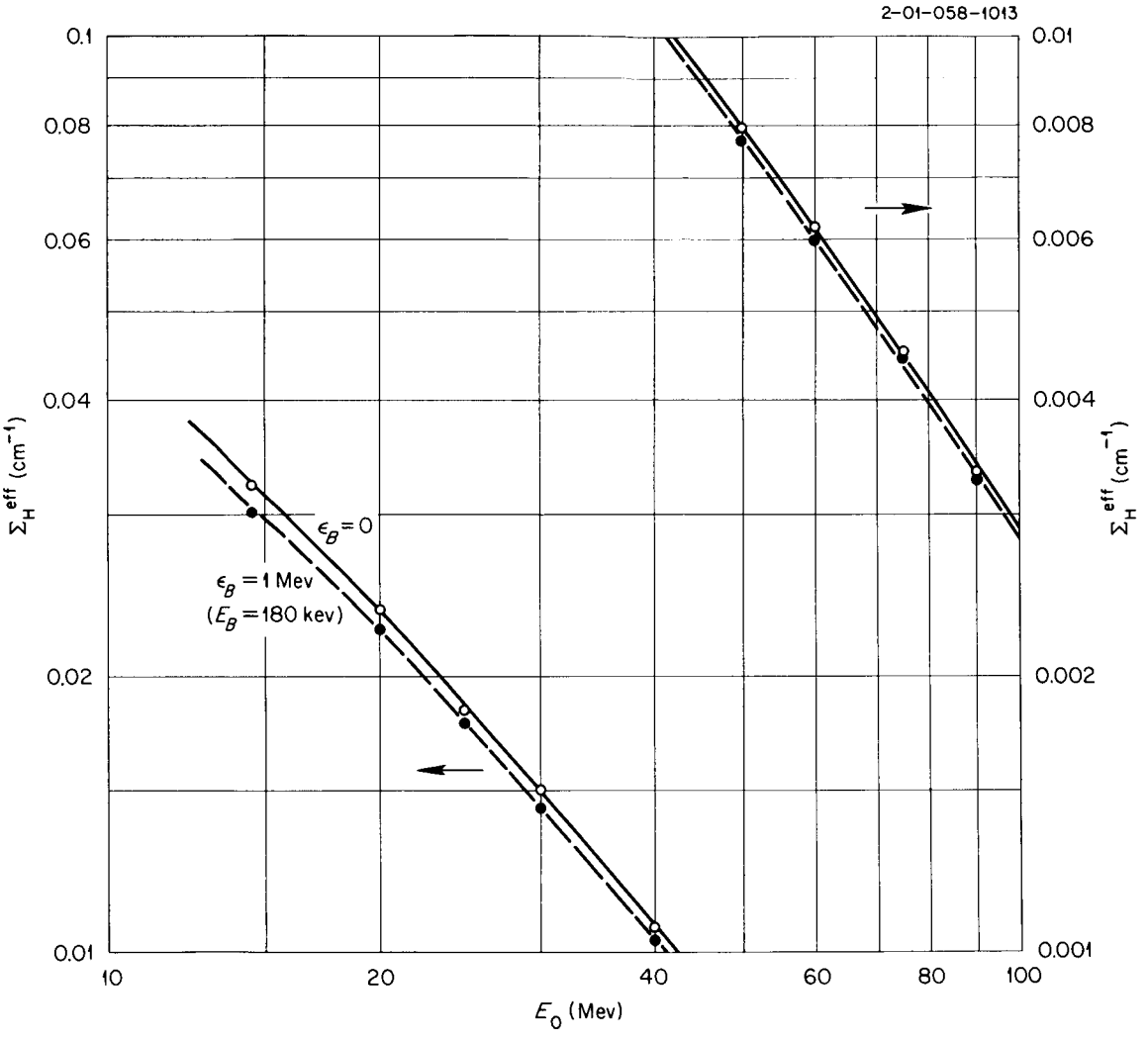

Fig. 10. Effective Macroscopic Cross Section Σ_H^{eff} for Elastic Neutron-Proton Scattering vs Neutron Energy (Plotted for Two Different Proton Biases ϵ_B).

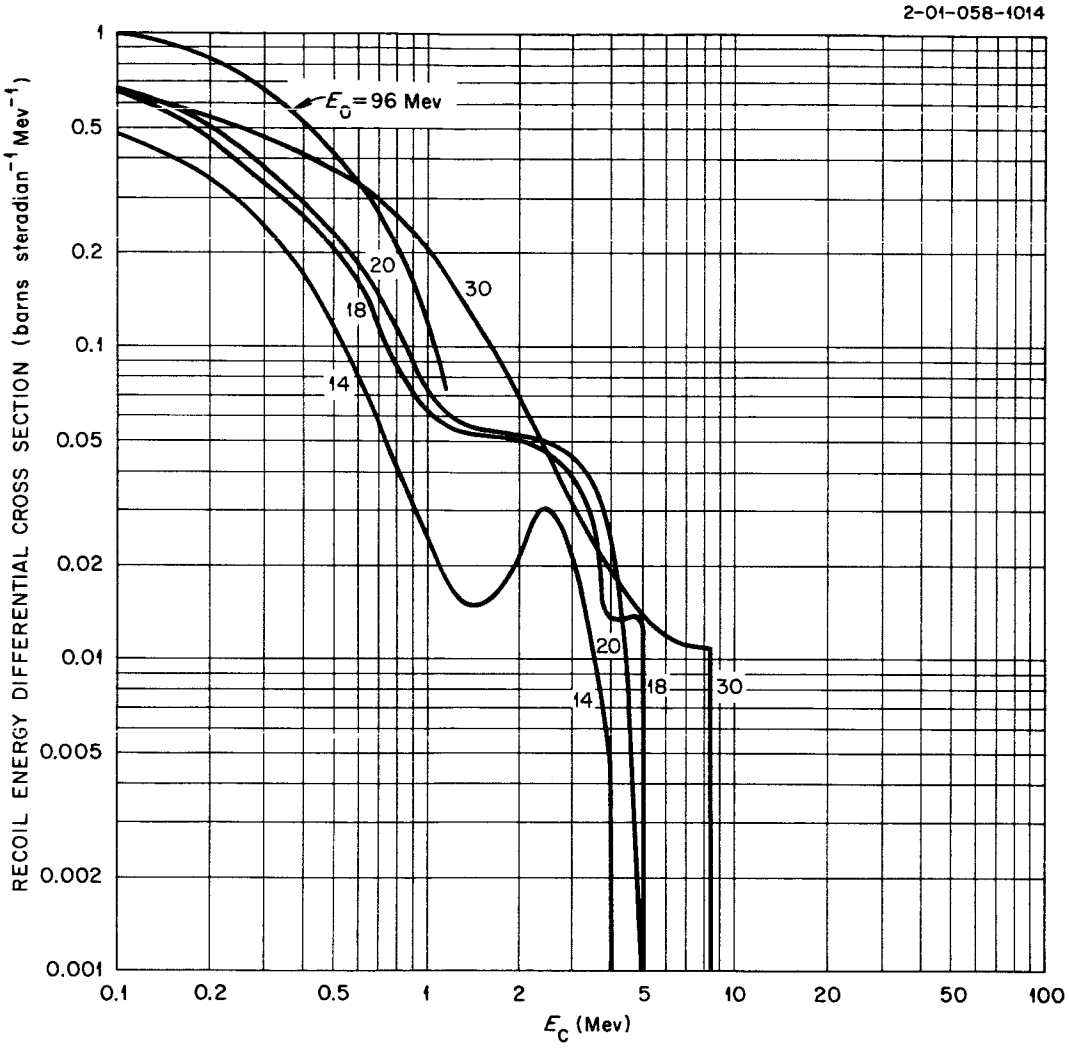

Fig. 11. Differential Cross Section for Elastic Scattering of Neutrons on Carbon as a Product of Carbon Recoil Energy.

used $F = 0.015\ E_C$ but from our calculation we find that $F = 0.01\ E_C$. Some recent data [27] show that F is even lower. We note then that the abscissa in Fig. 11 can be either E_C or $F = 0.01\ E_C$.

We can estimate the order of magnitude of the efficiency contribution from carbon recoils by a simplification similar to formula (25), i.e., by neglecting the finite resolution of the scintillator. This leads to the curves of Fig. 12a, where

$$\Sigma_C(E_o,\ \epsilon_B) = \int_{\epsilon_B}^{\infty} W_C(E_C)\ dE_C \qquad (30)$$

is plotted vs $E_B = 0.01\ \epsilon_B$ for some values of E_o. A comparison with the values of $\Sigma(E_o,\ \epsilon_B)$ plotted in Fig. 9 shows that this effect is negligible if ϵ_B is more than 10 MeV ($E_B > 100$ keV). However, if the resolution at very low energy is very broad, some carbon recoils can be counted above the bias. Figure 12b shows a plot for $E_o = 30$ MeV calculated from Eq. (9) for some values of $k^* = \frac{k}{\zeta^*}$ (parameter giving the resolution).

From inelastic collisions $C(n,n'\gamma)C$ there will be some carbon recoil energy, for which process the cross sections are less well known. For our calculation we assumed that the excitation functions of the mirror nuclei N_{13} and C_{13} are the same above 20 MeV:

$$\left[\frac{\sigma(\psi)}{\sigma}\right]_{N_{13}} = \left[\frac{\sigma(\psi)}{\sigma}\right]_{C_{13}} . \qquad (31)$$

In the center-of-mass system the respective excitation energies of the C_{13} and N_{13} nuclei in the reactions $n+C_{12} \rightarrow C_{13}$ and $p+C_{12} \rightarrow N_{13}$ are

$$E_C = \frac{A}{A+1}\ E_n + Q_n \qquad (32)$$

and

$$E_N = \frac{A}{A+1}\ E_p + Q_p . \qquad (33)$$

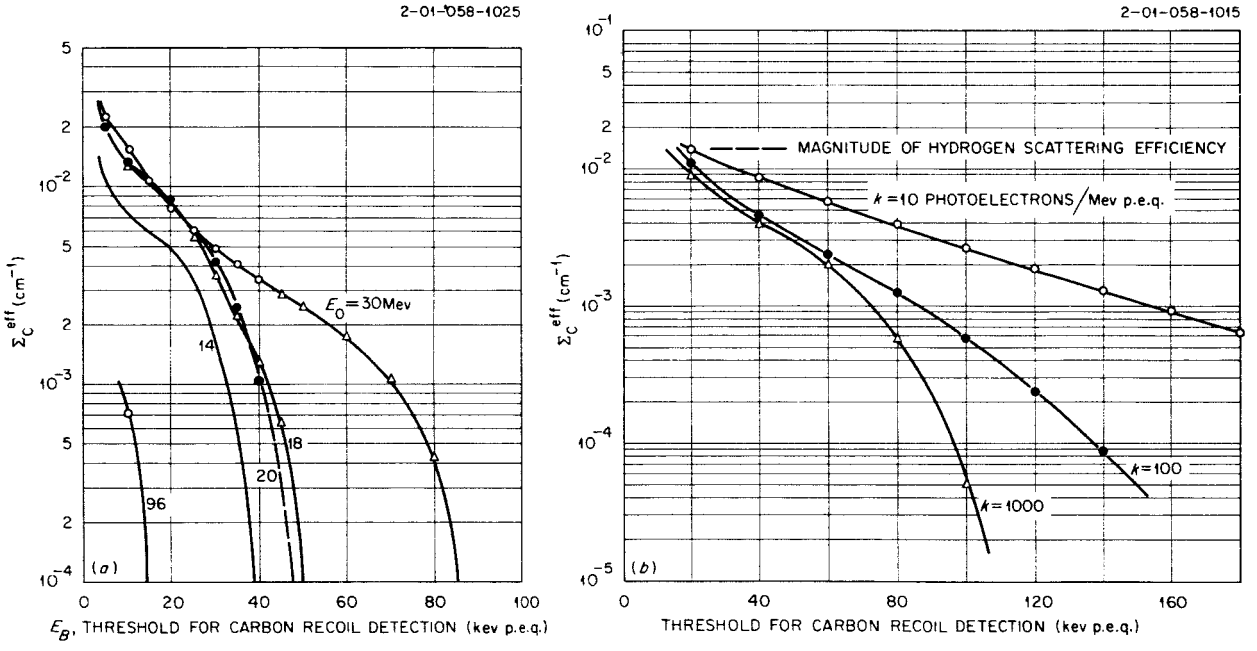

Fig. 12. Effective Macroscopic Cross Section Σ_C^{eff} vs Bias Setting for Detection of Elastic Carbon Recoils. (a) Data for different neutron energies and a perfect scintibloc and (b) data for E_0 = 30 MeV determined by the detector resolution (specified by the number of photoelectrons/ MeV p.e.q.).

Therefore we can use the C(p,p′)C* inelastic-scattering data with the relationship

$$E_n = E_p - 3.33 \text{ MeV} \tag{34}$$

and normalize so that

$$\int_{-1}^{+1} \sigma(\mu)\, d\mu = \sigma \ . \tag{35}$$

Figure 13, based on the same treatment as for the elastic scattering (Fig. 11), shows that the cross section is one-tenth that for elastic scattering. The main effect of these collisions is to remove 4.4-MeV energy from the incident neutron without changing its direction. This effect increases the probability of a collision with a hydrogen nucleus, and is included in the calculation related to the nonelastic scattering.

VIII. NONELASTIC SCATTERING: NATURE OF REACTION

The following reactions mainly compose the nonelastic cross section:

1. C(n,n′)C* leading to C* → 3α, Q = -7.281 MeV, but the lowest level leading to this decay is the 9.63-MeV level. The excitation increases rapidly between 12 and 15 MeV and remains nearly constant above this energy. Although a three-prong-star decay is not impossible, below 20 MeV the decay proceeds through the level near 10 MeV to the ground state of ^{8}Be (Refs. 28, 29). In the laboratory system in this threshold region this gives 3α particles which have energies in the range of 1 to 3 MeV; i.e., each particle gives a pulse of about 100 keV p.e.q. The spectrum of the light should be a very broad line centered at 300 keV. The efficiency resulting from this reaction is consequently very sensitive to the bias setting.

2. ^{12}C(n,p)^{12}B, Q = -12.592 MeV, and ^{12}C(n,np)^{11}B, Q = -18.721 MeV. The protons coming from these reactions are mostly above 1 MeV, and thus give important contribution to the efficiency.

3. ^{12}C(n,α)^{9}Be, Q = -5.709 MeV. Figure 4 shows the importance of this reaction, which gives a higher energy alpha particle than does the 3α decay.

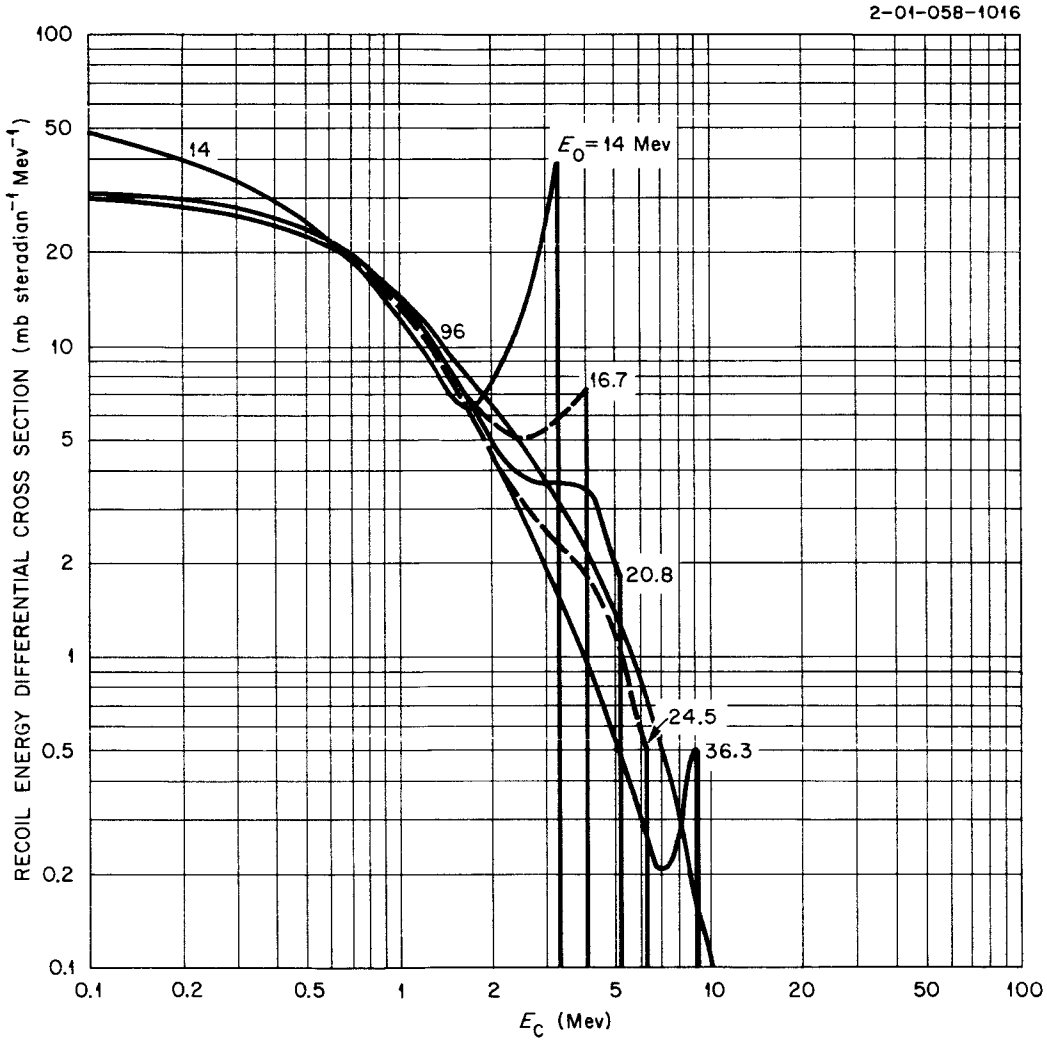

Fig. 13. Differential Cross Section for Inelastic Scattering of Neutrons on Carbon vs Carbon Recoil Energy for Excitation of 4.4-MeV Level.

IX. INTRANUCLEAR CASCADE MODEL

The determination of the efficiency needs not only the cross sections described above but also differential cross sections such as $\sigma(E_n \rightarrow E_n', E_p)$. For high values of E_n we use a method suggested by Fermi and developed by Serber[30] and Goldberger.[31] This method is called the "intranuclear cascade"[32,33] method, but a more appropriate term would be the "frozen nucleus" method, since it considers separately the interaction of the incoming particle and the secondary nucleons with the individual nucleons of the target nucleus. For practical use the nuclear potential and the spatial and momentum distribution of the target nucleons are those assumed to exist before the first interaction.

The validity of this method depends on the converse of the Bohr assumption[34] but in our case it may be made more plausible by the existence of some alpha-like structure inside the carbon nucleus. However, the application of this method to the interaction of 20-MeV neutrons on carbon caused considerable difficulties.

In previous cascade calculations it was assumed that the separation energy E_S was the same for all particles leaving the target, for example, $E_S = 7$ MeV. A more accurate calculation was suggested by the condition of validity of the method: the mean free path Λ must be greater than the channel radius R. In our case both are rather in the same order of magnitude, and some surface effect can occur. This surface effect should suppress, for example, an (n,p) reaction giving an emerging proton with an energy differing from the neutron energy by less than Q. This can be explained by saying that the wave number of a particle $k = \hbar^{-1}[2M(E+V)]^{\frac{1}{2}}$ is dramatically reduced when it reaches the surface.

We have made the assumption that the surface effect delays the time of emission of the particle sufficiently for the separation energy to be given by the potential of the compound nucleus (and not the initial nucleus). In this approximation we continue to neglect the changes in the nucleon density during the whole nuclear interaction. This assumption evidently suppresses the nonphysical processes, since empirical separation energies are employed. For example, for the

emission of the first particle we have $E_{S,n}(C_{13}) = 4.95$ MeV and $E_{S,p}(C_{13}) = 17.54$ MeV.

Practical Application

The analysis of the intranuclear cascade was made by the Monte Carlo method.[33] An incident neutron randomly strikes the "geometrical" cross section πR^2 (R = channel radius), and its mean free path is calculated as

$$\Lambda = (\sigma\rho)^{-1} , \qquad (36)$$

where σ is the nucleon-nucleon cross section as a function of the relative energy, and ρ is the nucleon density.

In the Bertini[33] program used here, ρ is assumed for simplicity to be uniform in each of three concentric regions. So, in a given region, Λ is a function only of the nucleon energy. The problem is now similar to a neutron transport problem in a finite geometry of three spherical regions.

By a series of random choices the further scattering of the primary and secondary nucleons is analyzed until they escape the nucleus or slow down to a cutoff energy which for convenience is chosen at 0.87 MeV for both protons and neutrons.

The particle type, energy, and momentum vector are recorded by Bertini's calculation on a magnetic history tape for each nucleon escaping the nucleus. It happens that the tape records are classified approximately by decreasing momentum magnitude. The tape does not give the time of particle escape, but in analyzing it we made the assumption that the lower the wave number, the more the surface effects can reflect the particle to delay the emission. So in the calculations employed here an analysis of the nuclear excitation energy is made after each particle emission record is read from the magnetic tape. If the excitation is positive, the record of the next escaping particle is studied, but if the excitation is negative, the cascade reaction is considered to have stopped before the emission in question. Excitation energies are obtained by use of nuclear mass tables.

The momentum and hence the energy of the recoil nucleus are also calculated and taken into account in determining the nuclear excitation.

Evaporation Process

After the emission of the last knock-on nucleon, the residual energy of the nucleus (E*) may be sufficiently high to boil off particles such as neutrons, protons, deuterons, tritons, ^{3}He, or alpha particles. We used the Dresner-Dostrovsky[35,36] method to compute this decay. First is computed the mean probability of emission of each type of particle (function only of E*, the separation energy E_S, and the Coulomb barrier energy). Then, after a random choice to determine which, if any, particle is to be evaporated, another choice gives the channel emission energy ϵ. At this point, since the nucleus velocity may be of the same order as the particle velocity, we say that if the direction of emission is randomly distributed the mean value (in the laboratory system) of the emitted particle square velocity is the sum

$$< v^2 > = v_C^2 + v_\epsilon^2 \ , \qquad (37)$$

where v_C is the velocity of the compound nucleus before decay and $v_\epsilon^2 = \frac{2\epsilon}{m}$ is the squared channel velocity. Similarly, we obtain the new v_C of the residual nucleus. The entire evaporation calculation is made again until all the probabilities of emission are given as zero. The mean residual energy is also given by the calculation.

It is in this way that the process computes the 3α decay of the excited C_{12} nucleus. This process proceeds via a ^{8}Be nucleus, and we considered the instability of its ground state (period $\sim 10^{-16}$ sec). Any ^{5}He and ^{5}Li nuclei were also forced to decay.

Multiple Scattering

The reactions with carbon may give rise to some neutrons among the reaction products. The lower their energy, the more likely they are to produce recoil protons. For each neutron leaving the target nucleus the mean escape path was calculated along with the mean free path Σ_H^{-1} corresponding to its energy.

If the neutron was a product of a cascade, the direction of emission was known and the average was made for all the points of the scintillator. If the neutron was evaporated, the average also included the direction of the axis. The probability of collision was then known and two random choices indicated, first, whether a collision had occurred and, second, what the energy of the recoil proton was. The result was an energy differential pseudo cross section.

Light Output

The result of the calculation was a set of histories in which an incident neutron may give one or more charged particles (including double-scattering pseudo reactions). Since we knew for each particle its light output, we calculated the light output from the incident neutron, i.e., the sum of the light output of each charged secondary or tertiary particle. Sorting these histories for each incident energy E_o gave the fast and total spectra of the light output as a function of the pseudo-electron equivalent threshold energy.

Results - Comparison with Experimental Data

Table 3 shows a comparison of the partial reaction cross sections estimated at 15 and 25 MeV. An item of some importance is the fact that we found no ground-state reactions (n,α) leading to ^9Be (see Section X). [Note: The excited levels of ^9Be lead to an evaporated neutron, in turn giving a contribution to the $(n,n'3\alpha)$ cross section.]

Light Spectrum Results

Due to the uncertainty in the light output from charged particles, our results on the fast spectrum data are more precise than for the total light. Figures 14 and 15 show the p.e.q. energy distribution of $\varphi(F)$, the fraction of the geometrical cross section, for two scintillator sizes. The integral of this function φ above a bias E_B, $\int_{E_B}^{\infty} \varphi(F)\, dF$, is the fraction of the geometrical cross section which contributes to the efficiency. With a finite resolution this integral is rather $\int_{E_B}^{\infty} \varphi(F)\, K(E_B,F)\, dF$ with a kernel $K(E_B, F)$ coming from

Table 3. Partial Reaction Cross Sections for Neutrons on Carbon

Reaction	Cross Sections (mb*) E_o = 15 MeV Experiment	E_o = 15 MeV Calculation	E_o = 25 MeV Experiment	E_o = 25 MeV Calculation
n,n′γ	220 ± 30	200 ± 20	95	73 ± 15
n,n′3α	320 ± 50	307 ± 20	240	230 ± 25
n,α	80 ± 20		50	
n,2n			6	8 ± 5
n,p		18 ± 6		15 ± 7
n,np			80	73 ± 15

*assuming a geometrical cross section πR^2 = 774 mb for the intranuclear cascade model nucleus.

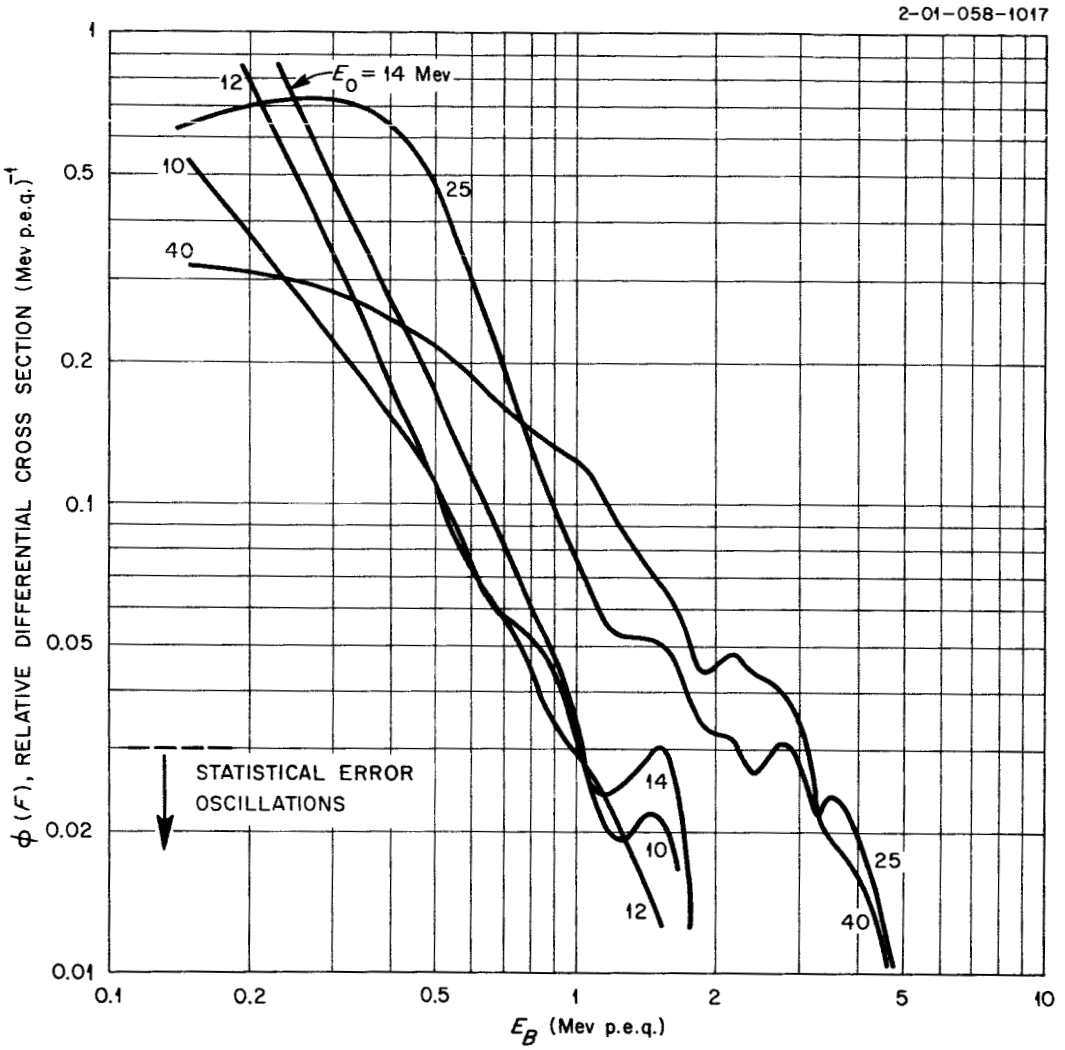

Fig. 14. Effective Relative Differential Cross Section $\varphi(F)$ vs Electronic Bias for 6.1-cm-thick Scintillator. The geometrical cross section is taken as 0.77 barn, and arises from cascade-plus-evaporation reactions in carbon. The results were smeared using K = 100 and $\zeta^* = 2$.

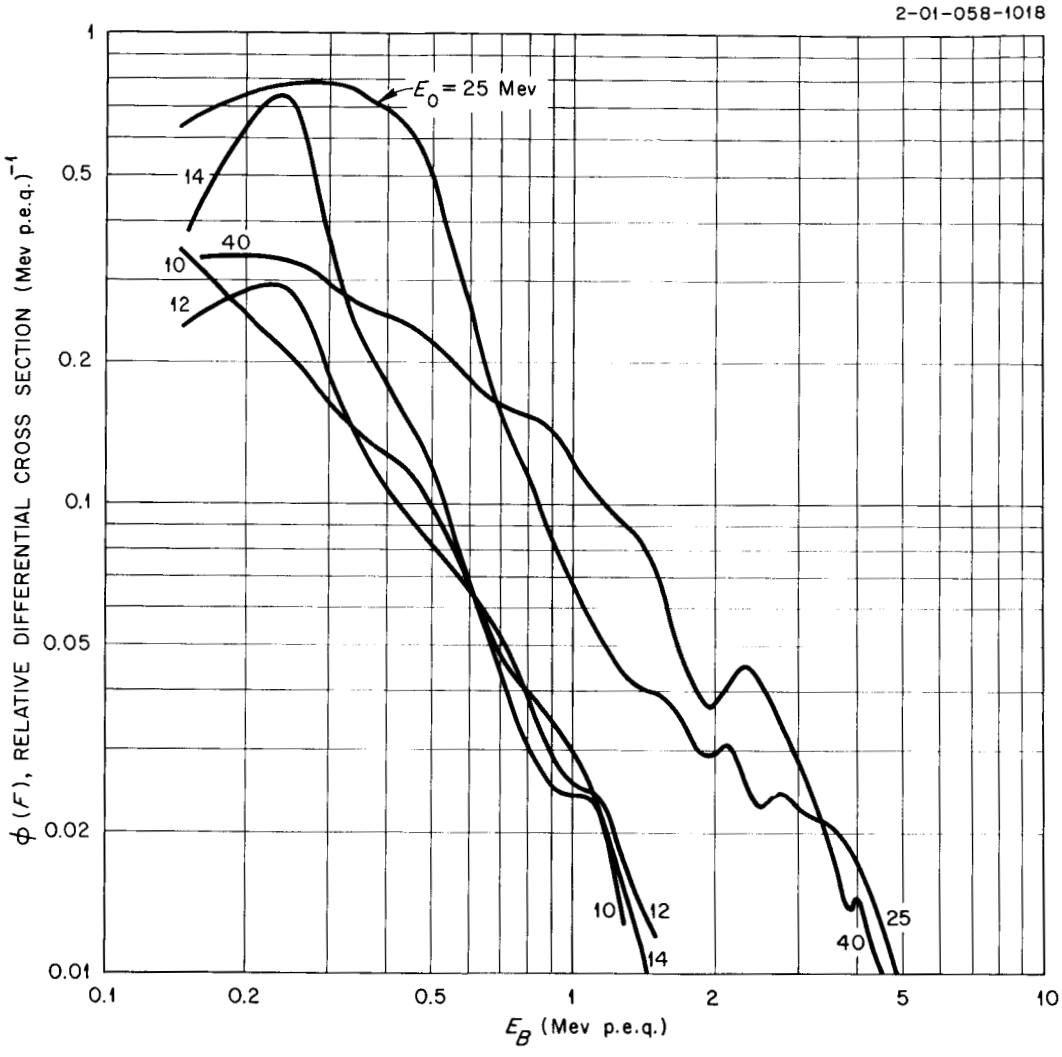

Fig. 15. Effective Relative Differential Cross Section $\varphi(F)$ vs Electronic Bias for 2.54-cm-thick Scintillator. The geometrical cross section is taken as 0.77 barn, and arises from cascade-plus-evaporation reactions in carbon. The results were smeared using K = 100 and $\zeta^* = 2$.

Eq. (9). The geometric cross section for carbon is here taken as 0.77 barn, corresponding to the lowest density portion of Bertini's nucleus. In other terms φ is also the efficiency cm^{-1} MeV^{-1} $(\Sigma_g)^{-1}$, where $\Sigma_g = N_C \sigma_g$ is the geometrical macroscopic cross section. We have estimated φ vs E, the p.e.q. energy.

Values of $\sigma_C^{eff} = \sigma_g \int_{E_B}^{\infty} \varphi(E)\, dE$ are tabulated in Table 4 for two scintillator sizes (h = 2.54 and 6.1 cm), with E_B taken equal to 180 keV p.e.q. (for K = 100 photoelectrons/MeV and $\zeta^* = 2$). These results are also plotted in Fig. 16, where it can be seen that the influence of size (double scattering) gave an increase of only 1% above E_o = 20 MeV but was more important for lower energies.

Figure 17 gives for E_o = 15 MeV the amplitude distribution per centimeter of the total-light spectrum from the cascade-plus-evaporation reaction, and for comparison the spectrum from first-order hydrogen scattering alone.

X. REACTION (n,α)

For the (n,α) reaction, which is not included in the intranuclear cascade process, we assume that the reaction products are isotropic in the center-of-mass system. Then the efficiency is

$$\eta_\alpha = h^* N_C \sigma_\alpha \frac{E_{\alpha max} - E_{\alpha,o}}{E_{\alpha max} - E_{\alpha min}} , \tag{38}$$

where σ_α is the total cross section for this reaction,[37-39] $E_{\alpha,o}$ is equal to the maximum value of $(\epsilon_B, E_{\alpha min})$, ϵ_B is the alpha-particle energy corresponding to the bias E_B, $E_{\alpha min}$ is the minimum possible alpha energy, and $E_{\alpha max}$ is the maximum energy of the alpha particle emitted. If we assume that only the neutron is relativistic, the momentum relation gives

$$\beta = \frac{V_{c.m.}}{c} = \frac{1}{A+1} \sqrt{\frac{E_o}{M_n c^2} \left(2 + \frac{E_o}{M_n c^2}\right)} \tag{39}$$

and

$$\frac{A}{A+1} E_o + Q = \left(1 + \frac{M_\alpha}{M_B}\right) E'_\alpha , \tag{40}$$

Table 4. Effective Cross-Section σ_C^{eff} at E_B = 180 keV p.e.q.

E_o(MeV)	σ_C^{eff} (mb)	
	For h = 6.1 cm	For h = 2.54 cm
10	94	65
12	128	91
14	187	150
15	207	168
20	319	313
25	326	320
30	334	331
40	310	307

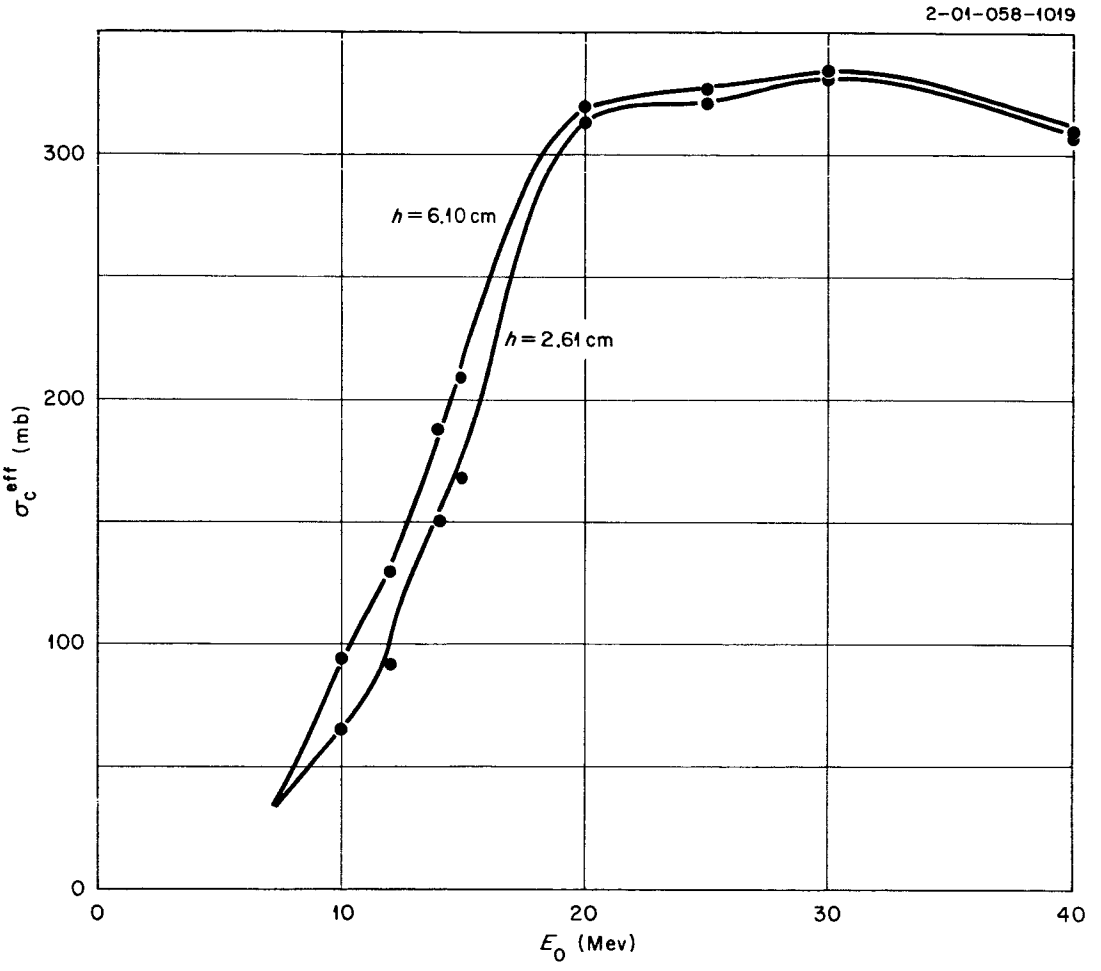

Fig. 16. Effective Microscopic Cross Section from Cascade vs Neutron Energy for Two Scintillator Thicknesses.

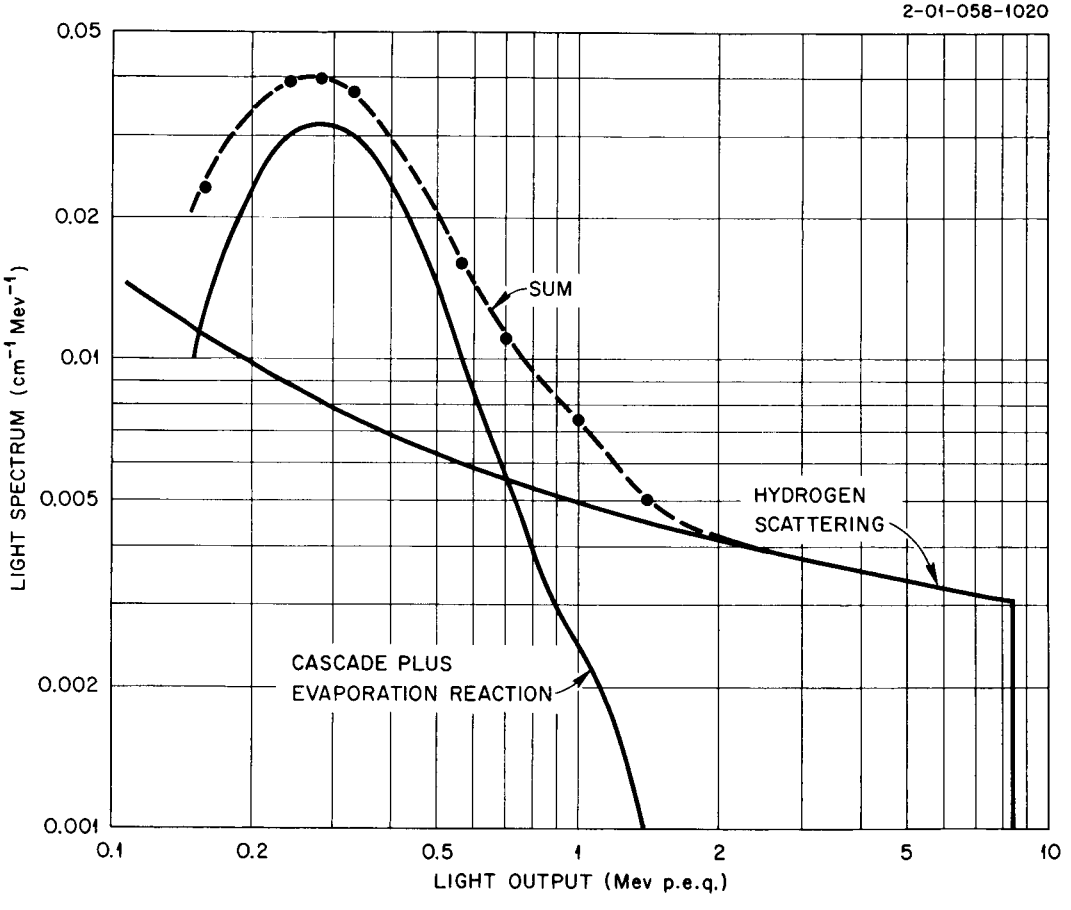

Fig. 17. Total Light Pulse-Height Spectra per Centimeter for 15-MeV Neutrons, from the Cascade-Plus-Evaporation Reaction and from Hydrogen Scattering.

where E'_α is the energy of the alpha particle in the center-of-mass system, $Q = -5.71$ MeV, and M_B is the mass of the ^{9}Be atom residual. Therefore

$$\left.\begin{matrix} E_\alpha^{max} \\ E_\alpha^{min} \end{matrix}\right\} = \tfrac{1}{2} M_\alpha \left(\sqrt{\frac{2E'_\alpha}{M_\alpha}} + V_{c.m.} \right)^2 . \qquad (41)$$

Values of E_α^{max} and F_α^{max} for some neutron energies are given in Table 5. It will be noted that this process has a smaller zero-bias efficiency than the $(n,n'3\alpha)$ reaction, but since only one alpha particle is emitted, the maximum light output is larger.

XI. SECOND-ORDER SCATTERING

As we have seen in Section IV [Eq. (10)], we may calculate the second-order efficiency η_2 by taking into account the "second effective collision":

$$\eta_2 = \frac{1}{J_o} \int_o^h dx \int_o^{E_o} \Phi_1(x,E) \left[\Sigma_H(E) g_H(E,E_B) + \Sigma_C(E) g_C(E,E_B)\right] dE . \qquad (42)$$

We also should note that when we have integrated the spectrum shown in Fig. 15 the differential cross section of the reaction $C(n,n'\gamma)C$ calculated by the cascade is distributed as the result of the free neutron-nucleon interaction and not forward-peaked like the observed inelastic scattering shown in Fig. 13 (even if the total cross section is correct). So although this second-order scattering is included in the cascade calculation, we have to add a "forward-peak flux" in the calculation of the second-order scattering and subtract terms corresponding to the incorrect angular distribution. From these considerations Φ_1 is the sum of two terms:

$$\Phi_1 = \Phi_H(x,E) + \Phi_i^*(x,E) . \qquad (43)$$

The first one results from undetected first scattering with hydrogen, and since this scattering is nearly isotropic,

Table 5. Energy and Fast-Light Output Extrema from $^{12}C(n,\alpha)^{9}Be$

E_o (MeV)	E_α^{max} (MeV)	F_α^{max} (MeV)	E_α^{min} (MeV)	F_α^{min} (MeV)
14.5	8.36	0.55	2.95	0.12
25	18.0	1.8	7.27	0.43
50	40.8	7	18.6	1.9
75	63.8	14	27.8	3.8
100	86.8	23	38.1	6.1

$$\Phi_H = J_1^H(x,E_o)\ \varphi_1(E,E_o) \tag{44}$$

with $\varphi_1(E) = 1/E$ for $E_o-\epsilon_B < E < E_o$, $\equiv 0$ otherwise; J_1^H is the current of hydrogen-scattered neutrons (in a one dimensional approximation) with this variable separation. The contribution η_2^H of Φ_H to η_2 is again the product of two terms:

$$\eta_2^H = \left[\frac{1}{J_o}\int_o^h J_1^H(x)\ dx\right]\int_o^{E_o} \varphi_1(E)\ \Sigma_1^{eff}(E,\epsilon_B')\ dE$$

$$\equiv \left[\frac{1}{J_o}\int_o^h J_1^H(x)\ dx\right]\Sigma_{2,H}^{eff}\ . \tag{45}$$

The effective cross section here is a function of ϵ_B' because the light from any second collision will add to the light from the first. In the preceding sections we have already calculated the first-effective-collision macroscopic cross section for several energies E_o with bias ϵ_B:

$$\Sigma_1^{eff}(E_o,\epsilon_B) = \Sigma_H^{eff}+\Sigma_C^{eff}\ . \tag{46}$$

A look at the variation of Σ_1^{eff} vs E_o (see the final results plotted in Fig. 18 and data in Ref. 5) shows that since η_2 is only a corrective term the mean value $<\Sigma_1^{eff}>$ taken between $E_o-\epsilon_B$ and E_o is not too different from $\Sigma_1^{eff}(E_o)$. To calculate $\Sigma_1^{eff}(E_o,\epsilon_B')$, we made the additional assumption that the variation with ϵ_B' is similar to that of Σ_H^{eff} as given by Eq. (26); therefore

$$\Sigma_1^{eff}(E_o,\epsilon_B') = \Sigma_1^{eff}(E_o,\epsilon_B)\ \frac{1-\alpha(E_o)\ \frac{\epsilon_B'}{E_o}}{1-\alpha(E_o)\ \frac{\epsilon_B}{E_o}}$$

$$\cong \Sigma_1^{eff}(E_o,\epsilon_B)\left[1-\alpha(E_o)\ \frac{\epsilon_B'-\epsilon_B}{E_o}\right]\ . \tag{47}$$

If the light output were a linear function of proton energy, the mean

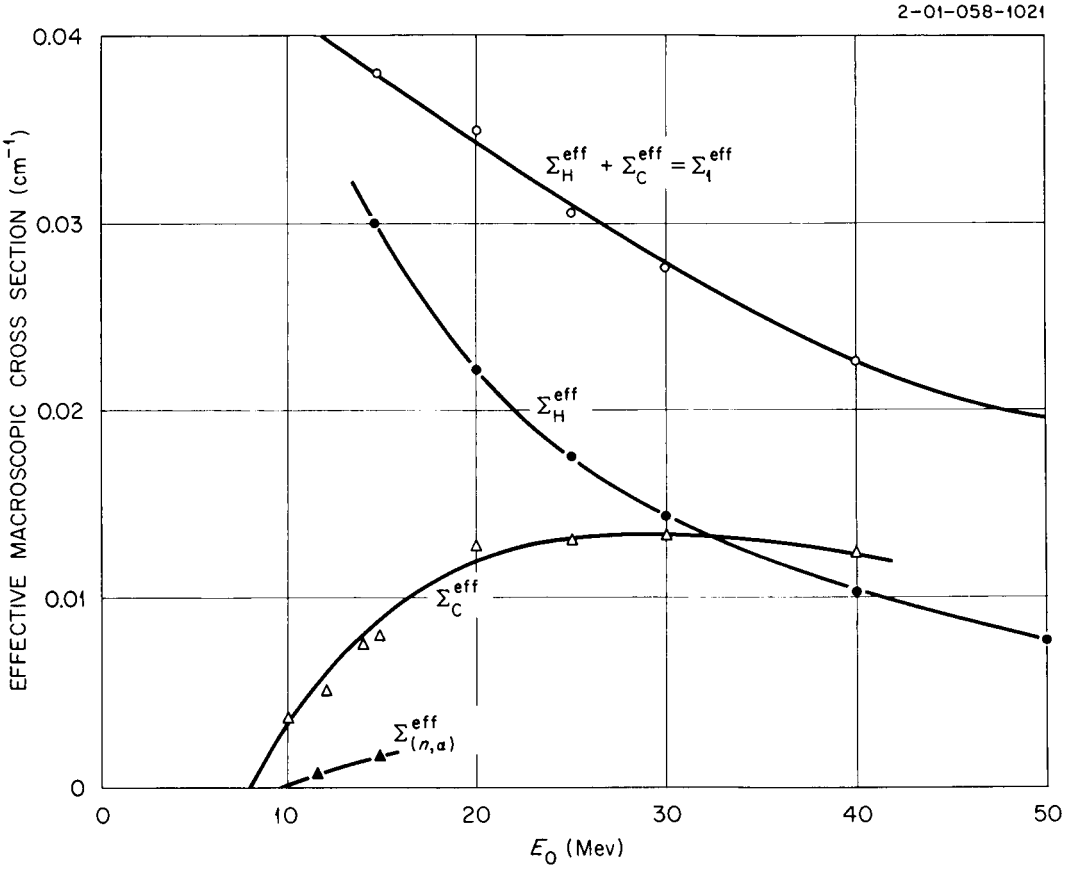

Fig. 18. First-Collision Effective Macroscopic Cross Sections as a Function of Neutron Energy for h = 6.1 cm and E_B = 180 keV.

value $\bar{\epsilon}'_B = \frac{1}{2}\,\epsilon_B$. If the relation illustrated in Fig. 19 were quadratic $\bar{\epsilon}'_B = \frac{\pi}{4}\,\epsilon_B$. As a compromise, we used $\bar{\epsilon}'_B = \frac{2}{3}\,\epsilon_B$. Within these approximations the second term of Eq. (45) becomes

$$\Sigma_{2,H}^{eff} \equiv \int_o^{E_o} \varphi_1\, \Sigma_1^{eff}(E,\epsilon'_B)\, dE$$

$$= \Sigma_1^{eff}(E_o,\epsilon_B)\, [1+\tfrac{1}{3}\alpha(E_o)\, \epsilon_B/E_o]\, \epsilon_B/E_o \ . \qquad (48)$$

Let us now consider the effect of the forward-peaked flux in Eq. (43), which flux may be written

$$\Phi_i^* = J_1^i(x,E_o)\, \delta(E-E_i) \ , \qquad (49)$$

with $E_i = E_o - 4.43$ MeV. According to Section IV, however, most of the neutrons in Φ_i^* were analyzed in Section IX. Therefore, if we make the hypothesis that the cascade gives a "white spectrum,"

$$\frac{\partial \eta_2^i}{\partial x} = \frac{J_1^i}{J_o} \left[\delta(E-E_i)\, \Sigma_1^{eff}(E,\epsilon_B)\, dE - \int_o^{E_i} \frac{1}{E_i}\, \Sigma_H(E)\, g_H(E,E_B)\, dE \right] . \qquad (50)$$

The term between the brackets is equal to

$$\Sigma_1^{eff}(E_i,\epsilon_B) - \left\langle \Sigma_1^{eff}(E,\epsilon_B) \right\rangle_o^{E_i} + \int_o^{E_i} \frac{1}{E_i}\, \Sigma_C(E)\, g_C(E,E_B)\, dE \ , \qquad (51)$$

and the first two terms cancel in the same approximation used for η_2^H, giving

$$\int_o^{E_i} \frac{\Sigma_C(E)\, g_C(E,E_B)\, dE}{E_i} \ . \qquad (52)$$

It will be convenient to let Eq. (52), which corresponds to two consecutive carbon collisions, be equal to

$$\omega(E_i,E_B)\, \Sigma_{2,H}^{eff} \ , \qquad (53)$$

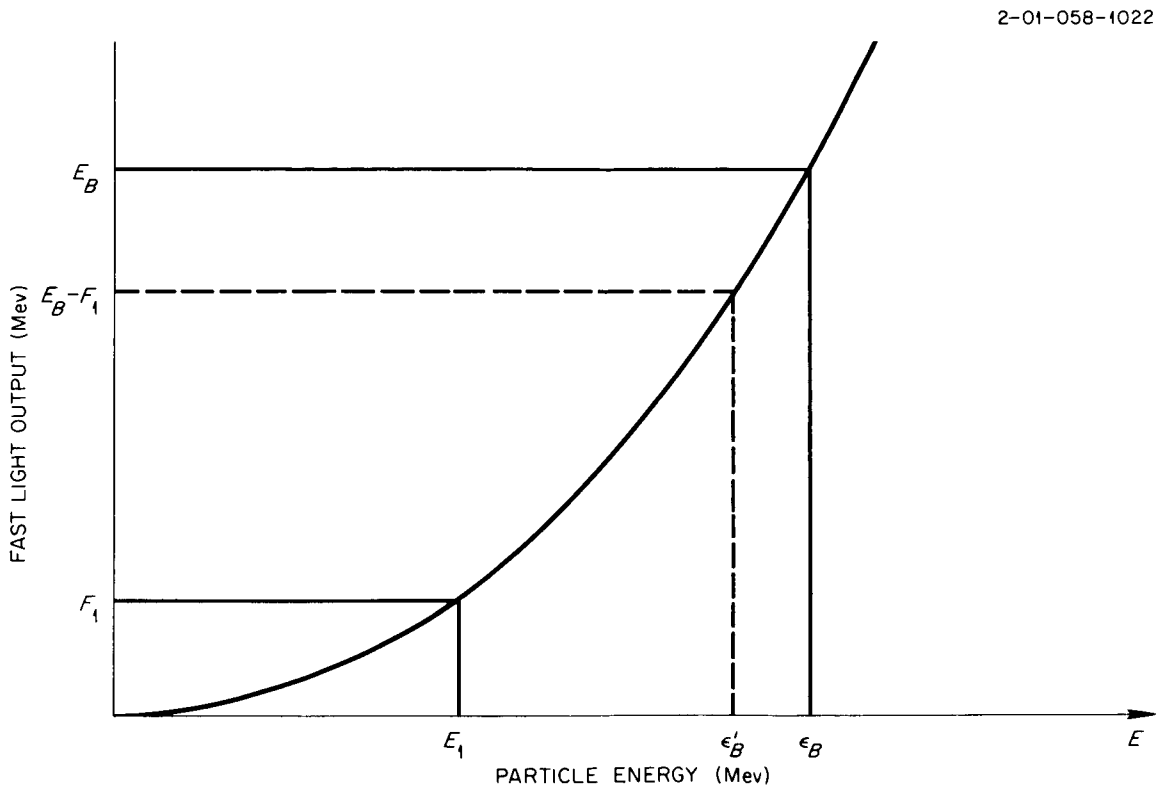

Fig. 19. Influence of the First Collision on the Bias for Detection of the Second Collision (Both Are Assumed To Be n-p Scattering).

so that by defining the usual effective cross section we can write

$$\omega \equiv \frac{\int_0^{E_i} \Sigma_C^{eff}(E)\, dE}{E_i\, \Sigma_{2,H}^{eff}} . \tag{54}$$

We approximate the integral in Eq. (54) as

$$\Sigma_C^{eff}(E_o) \int_{\epsilon_B+Q_p}^{E_i} dE = \Sigma_C^{eff}(E_o)(E_i - Q_p - \epsilon_B) \tag{55}$$

if $E_i > \epsilon_B+Q_p$ or equal to zero if $E_i < \epsilon_B+Q_p$ [Q_p = 12.6 MeV is the energy deficit in the $^{12}C(n,p)$ reaction, and the Monte Carlo results show a low cascade contribution below about this incident energy]. So if $E_i > \epsilon_B+Q_p$ and ϵ_B/E_o is small, the definition of $\Sigma_{2,H}^{eff}$ in Eq. (48) gives

$$\omega = \frac{E_o\, \Sigma_C^{eff}(E_o)}{\epsilon_B\, \Sigma_1^{eff}(E_o)} \left[1 - \frac{Q}{E_i} - \frac{\epsilon_B}{E_i} - \frac{\epsilon_B\, \alpha(E_o)}{3\, E_o}\right]. \tag{56}$$

We can now obtain η_2 from a combination of Eqs. (45), (50), and (53):

$$\begin{aligned} \eta_2 &= \left\{\frac{1}{J_o}\int_o^h \left[J_1^H(x) + \omega(E_i,E_B)\, J^i(x)\right] dx\right\} \Sigma_{2,H}^{eff} \\ &\equiv \left[\frac{1}{J_o}\int_o^h J_1(x)\, dx\right] \Sigma_{2,H}^{eff}(E_o) , \end{aligned} \tag{57}$$

where we must recall that $\omega = o$ if $E_i < \epsilon_B+Q_p$, or equivalently $E_o < \epsilon_B+16.9$ MeV. For evaluating the first term, $h_2^* \equiv \frac{1}{J_o}\int_o^h J_1(x)\, dx$, observe that J_1 is related to the primary current $J(x) = J_o e^{-\Sigma_R x}$ by

$$\frac{dJ_1}{dx} = \Sigma_t\, J - \Sigma_R'(E)\, J_1 , \tag{58}$$

where Σ_R' is the removal cross section for energy E, and Σ_t is the

transport cross section defined below. The solution is

$$J_1 = \frac{\Sigma_t}{(\Sigma_R' - \Sigma_R)} J_o \left(e^{-\Sigma_R x} - e^{-\Sigma_R' x}\right) , \tag{59}$$

and

$$h_2^* = \frac{\Sigma_t}{(\Sigma_R' - \Sigma_R)} \left[\frac{1}{\Sigma_R'} \left(e^{-\Sigma_R' h} - 1\right) - \frac{1}{\Sigma_R} \left(e^{-\Sigma_R h} - 1\right)\right]$$

$$\cong \tfrac{1}{2} h^2 \Sigma_t, \text{ independent of } \Sigma_R' \text{(and E)}. \tag{60}$$

The cross section for the transport $J \rightarrow J_1$ is $\Sigma_t = \Sigma_H + N_C \omega \sigma_i$, $= \Sigma_H + \Sigma_i \omega$. Therefore

$$\eta_2 = \tfrac{1}{2} h^2 \Sigma_t \Sigma_{2,H}^{eff}$$

$$= \tfrac{1}{2} h^2 (\Sigma_H + \Sigma_i \omega) \frac{\epsilon_B}{E_o} \Sigma_1^{eff}(E_o) \left[1 + \tfrac{1}{3} \frac{\epsilon_B}{E_o} \alpha(E_o)\right] . \tag{61}$$

XII. COMPARISON WITH EXPERIMENTAL DATA AT 14.45 MeV

The efficiencies calculated for scintillators B_1 and B_2 (h = 2.61 and 6.10 cm, respectively)at threshold values E_B = 180 and 1800 keV p.e.q. are itemized below as an example, and then compared against experimental values.

Figure 20 illustrates the energy vs light output relationship described in Section II. From Fig. 20 one may see that E_B = 0.18 and 1.8 MeV p.e.q. correspond to proton energies E_B = 1.05 and 5.3 MeV.

The two scintillators of thickness 2.61 and 6.1 cm have effective thicknesses h_1^* and h_2^* of 2.43 and 5.15 cm, based on a removal cross section Σ_R = 0.0567 cm^{-1}.

In all cases here the estimated edge effect loses counts from about 0.0017 of all neutrons incident, based from Fig. 8 either on 2.2% of an unbiased hydrogen efficiency of 0.08 for the B_1 detector or on 1% of 0.17 for the B_2 detector. It will be recalled that this edge effect is based on the E_{psd} threshold value.

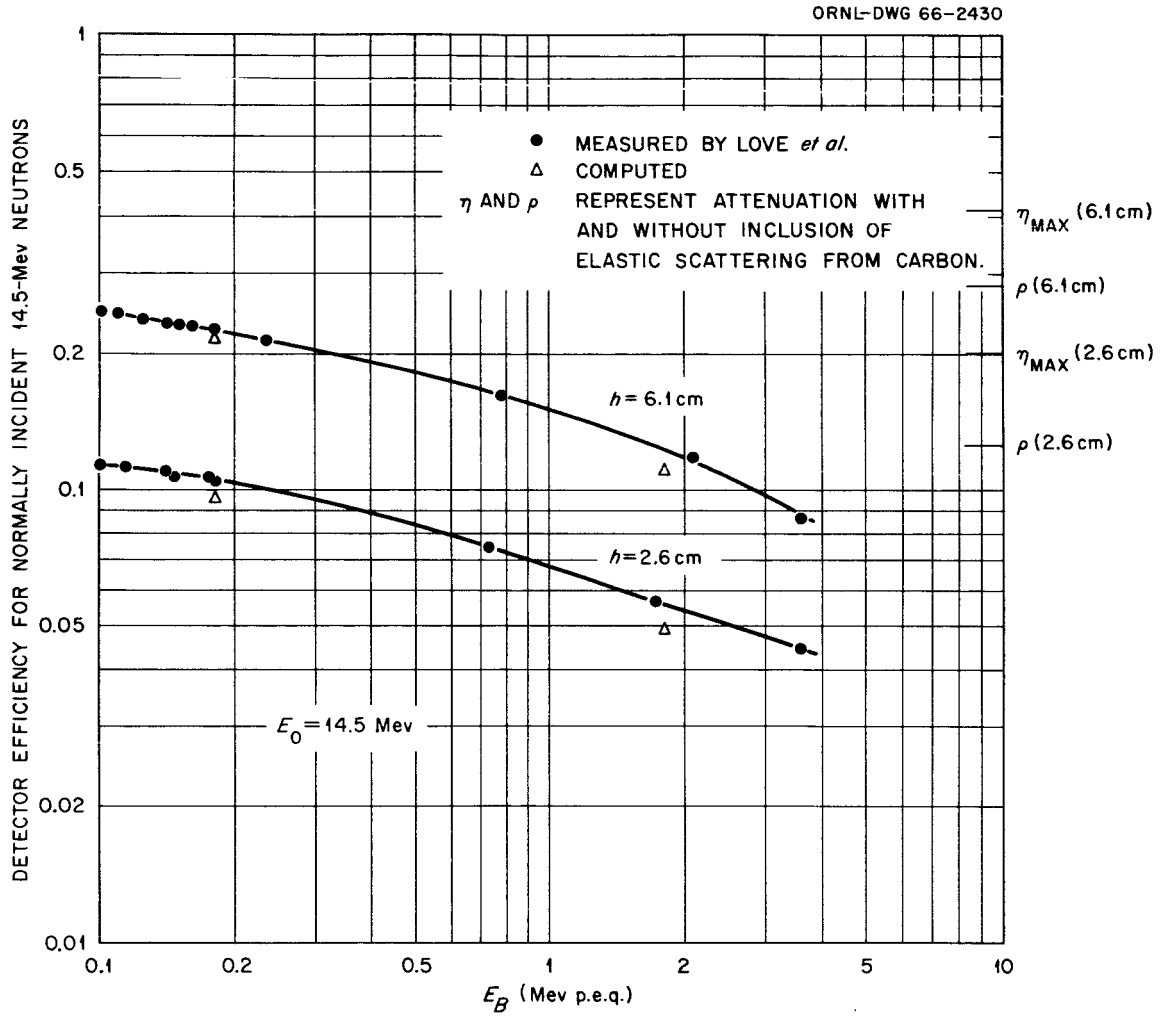

Fig. 20. Experimental and Calculated Detection Efficiencies for Various Fast-Light Thresholds, E_B, Compared with Results for η and ρ Taken from Fig. 2.

Estimates for E_B = 180 keV p.e.q.

Hydrogen Scattering. -- Σ_H = 0.03233 cm^{-1}; α/E_o = 0.0716; therefore Σ_H^{eff} = 0.0300. The contributions to η are 7.29 and 15.5% for the 2.6- and 6.1-cm detectors; or with edge effect considered at the 2-MeV E_{psd} threshold, 7.1 and 15.3%, respectively.

Cascade from Table 5. -- σ_C = 160 and 200 mb for thin and thick detectors, giving Σ_C^{eff} = 0.0064 and 0.0079, and the efficiency contributions from carbon reactions become 1.56 and 4.1%, respectively.

$(n,\alpha)^9$Be Reactions. -- For this energy E_α^{max} = 8.4 MeV, E_{min} = 2.9 MeV, and σ = 80 mb. From Fig. 20, ϵ_B^α = 4 MeV and Σ_α^{eff} = 0.0025. So the contributions are 0.6 and 1.3% to the 2.6- and 6.1-cm efficiencies.

Second Order. -- σ_i = 220 mb, E_i = 10 MeV, and ω = 0; so Σ_t = 0.03233. $\Sigma_{2,H}^{eff}$ = 0.0027 and 0.0028. h_2^* = 0.113 and 0.61 cm, respectively. The efficiency contributions are 0.03 and 0.17%.

$(n,n'\gamma)$ Gamma Detection. -- σ_i = 220 mb and gamma-detection efficiencies at zero bias may be estimated at 10 and 15%, respectively, for the distributed source. Thus without pulse-shape discrimination the gamma-detection contributions are about 0.2 and 0.6%, respectively, and almost half this with pulse-shape discrimination and E_{psd} = 2.MeV.

Total. -- η = 9.4% for the 2.61-cm detector and 21.2% for the 6.1-cm detector with pulse-shape discrimination (and thus edge effects) or 9.7 and 21.7% without.

Estimates for E_B = 1800 keV p.e.q.

Hydrogen Scattering. -- Σ_H^{eff} = 0.0201. The contributions are 4.86 and and 10.4% with the edge effect ignored, and 4.7 and 10.2% with edges effect included.

Cascade from Fig. 15. -- σ_C = 0.

$(n,\alpha)^9$Be Reactions. -- From Fig. 20 $\epsilon_B^\alpha \sim$ 18 MeV, so Σ_α^{eff} = 0.

Second Order. -- $\Sigma_{2,H}^{eff}$ = 0.0085. The contribution η_2 = 0.1 and 0.5%.

$(n,n'\gamma)$ Gamma Detection. -- About 0.1 and 0.3% as above.

Total. -- η_2 = 4.9 and 11.0%, counting edge effect, for the 2.6- and 6.1-cm detectors. Unvertainties would be no more than a few percent if the underlying cross-section uncertainties dominated. Effects of errors in the light output relation are presently difficult to estimate.

Table 6 and Fig. 21 compare the above results with the experimental values of Love et al.[40] The experimental values were obtained with a detector system which included a plastic light pipe and a 0.5-cm plastic anticoincidence scintillator between the detector and the neutron source. Monte Carlo calculations[41] employed to estimate the implied small corrections indicated that in both cases the nearby plastic increased the detector efficiency by a factor of 1.01 ± 0.01 at the high bias and 1.02 ± 0.007 at the low bias. These corrections were not included because of their small importance and questionable magnitudes. The estimates in Table 6 do not include pulse-shape discrimination because the comparable experimental values suffered from an obvious loss of low-energy neutron pulses.

Examination of Table 6 shows that the estimates at the higher threshold are low by 13% or so, which could most easily occur if there were some difficulty with the estimation of light output for protons. This should have little effect at the lower bias, where estimates are low by an average of 5%. The latter discrepancy seems not fully accounted for by neglect of the effects of the surrounding materials. The agreement at low bias is sufficiently good to suggest that the main effects have been taken into account in the analysis; if, however, experimental cross sections become known in detail forthe carbon reactions, over the energy range of interest, it will be more exact to estimate efficiencies by direct application of Monte Carlo techniques.

Table 6. Comparison of Calculated and Experimental Values for 14.5-MeV Neutron[a]

Scintillator Thickness (cm)	Bias Threshold (keV p.e.q.)	Experimental Efficiency[b]	Calculated Efficiency
2.61	180	0.105 ± 0.001	0.097
	1800	0.055 ± 0.001	0.049
6.10	180	0.226 ± 0.002	0.217
	1800	0.123 ± 0.003	0.110

[a]The effect of the ~ 3-cm plastic light pipes and the 0.5-cm plastic anticoincidence counter has been ignored (see text). The values given here correspond to the case without pulse-shape discrimination. Short-range interpolations have been employed among the experimental data, causing the uncertainties in the experimental values to be increased.

[b]T. A. Love et al., Neutron Phys. Div. Ann. Progr. Rept. Aug. 1, 1964, ORNL-3714, Vol. II, p. 93; see also ORNL-3893 (in press).

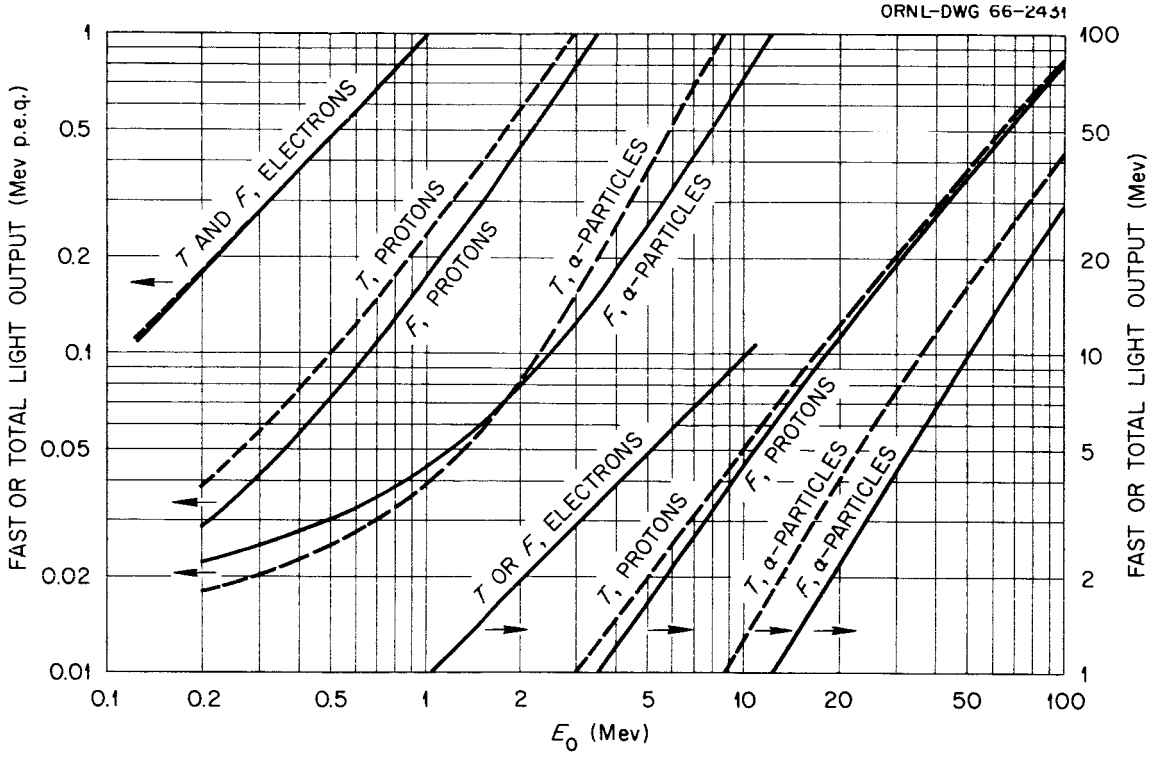

Fig. 21. Fast- and Total-Light Output, F and T, for Electron, Proton, and Alpha Particles. The electron data are from Flynn et al. (Ref. 21). The formulation for alpha particles and protons is given in Section II.

ACKNOWLEDGMENTS

I wish first to thank E. P. Blizard and F. C. Maienschein of the Neutron Physics Division for accepting me for a one-year visit and for the considerable help they gave me, and to thank J. Bourgeois, head of the Department d'Etudes des Piles at the French AEC, who gave me the grant for this year's work. Also, I am greatly indebted to R. W. Peelle, with whom I worked, for helping me every day during this project and later for helping me to write this paper, to L. Dresner and H. Bertini for explaining their evaporation and cascade program to me, and finally, to all the people of the Bulk Shielding Facility, particularly T. A. Love and R. T. Santoro, for their kind help.

REFERENCES

1. R. Batchelor et al., Nucl. Instr. Methods 13, 70 (1961).
2. J. E. Hardy, Rev. Sci. Instr. 29, 705 (1958).
3. H. W. Broek and C. E. Anderson, Rev. Sci. Instr. 31, 1063 (1960).
4. H. Grässler and K. Tesch, Nucl. Instr. Methods 10, 353 (1961).
5. R. J. Kurz, A 709/7090 Fortran-II Program to Compute the Neutron-Detection Efficiency of Plastic Scintillators for Neutron Energies from 1 to 300 MeV, UCRL-11339 (1964).
6. R. W. Peelle et al., Neutron Phys. Div. Ann. Progr. Rept. Aug. 1, 1963, ORNL-3499, Vol. II, p. 73.
7. W. A. Gibson et al., op. cit., ORNL-3499, Vol. II, p. 109.
8. J. A. Draper, Rev. Sci. Instr. 25, 558 (1959).
9. C. E. Wiegand et al., Rev. Sci. Instr. 33, 526 (1962).
10. L. Cranberg, R. K. Beauchamp, and J. S. Levin, Rev. Sci. Instr. 28, 89 (1956).
11. R. W. Owen, Trans. IRE NS-5, 198 (1958).
12. R. J. Schuttler, The Saturation Relation for Slow Light with Specific Energy Loss from Charged particles in Deoxygenated Liquid Organic Scintillators (to be published).
13. T. J. Gooding and H. G. Pugh, Nucl. Instr. Methods 7, 189 (1960).
14. H. C. Evans and R. H. Bellamy, Proc. Phys. Soc. 74, 483 (1959).
15. J. B. Birks, Proc. Phys. Soc. A64, 74 (1952).
16. C. J. Taylor et al., Phys. Rev. 84, 1034 (1951).
17. H. B. Frey et al., Phys. Rev. 82, 372 (1951).
18. G. T. Wright, Phys. Rev. 91, 1282 (1953).
19. D. L. Horrocks, Rev. Sci. Instr. 34, 1035 (1963).
20. J. B. Birks, Trans. IRE NS7, 2 (1960).
21. K. F. Flynn et al., Nucl. Instr. Methods 27, 13 (1964).
22. G. Walter et al., J. de Physique 24, 1017 (1963).
23. T. A. Love and R. J. Schuttler, Neutron Phys. Div. Ann. Progr. Rept. Aug. 1, 1964, ORNL-3714, Vol. II, p. 136.
24. B. V. Rybakov and V. A. Sidorov, "Fast Neutron Spectroscopy", Supplement No. 6 to Soviet Journal on Atomic Energy (1958), translation by Consultants Bureau, New York, 1960.
25. B. Rossi and G. Staub, Ionization Chambers and Counters, McGraw-Hill, New York, 1951.
26. J. L. Gammel, Chapter V, p. 2209, Part II of Fast Neutron Physics, J. B. Marion and J. L. Fowler, ed., Interscience, New York, 1963.

27. V. V. Verbinski et al., Neutron Phys. Div. Ann. Progr. Rept. Aug. 1, 1964, ORNL-3714, Vol. I, p. 79.

28. G. M. Frye, Jr., L. Rosen, and L. Stewart, Phys. Rev. 99, 1375 (1955).

29. J. D. Jackson and D. I. Wanklyn, Phys. Rev. 90, 381A (1953).

30. R. Serber, Phys. Rev. 72, 1114 (1947).

31. M. L. Goldberger, Phys. Rev. 76, 1269 (1948).

32. W. Horning and L. Baumoff, Phys. Rev. 75, 370 (1949).

33. H. Bertini, Phys. Rev. 131, 1801 (1963); also Monte Carlo Calculations on Intranuclear Cascades, ORNL-3383 (1963).

34. J. M. Blatt and V. F. Weisskopf, Theoretical Nuclear Physics, 4th ed., Wiley, New York, 1959.

35. L. Dresner, EVAP - A Fortran Program for Calculating the Evaporation of Various Particles from Excited Compound Nuclei, ORNL-TM-196 (1961).

36. I. Dostrovsky, Z. Fraenkel, and P. Rabinowitz, Phys. Rev. 118, 791 (1960).

37. D. J. Hughes and R. S. Schwartz, Neutron Cross Sections, Vol. 1, 2nd ed., BNL-325 (July 1, 1958).

38. E. A. Davis et al., Disintegration of O^{16} and C^{12} by Fast Neutrons, submitted for publication to Nucleur Physics.

39. M. L. Chatterjee and B. Sen, Nucl. Phys. 51, 583 (1964).

40. T. A. Love et al., Neutron Phys. Div. Ann. Progr. Rept. Aug. 1, 1964, ORNL-3714, p. 134, Vol. II, and Absolute Efficiency Measurement of Ne-213 Organic Phosphors for the Detection of 14.4- and 2.6-MeV Neutrons, ORNL-3893 (in press).

41. R. T. Santoro et al., Effects of Plastic Layers and Light Pipes on the Efficiency of Organic Neutron Scintillators, ORNL-3892 (to be published).